TU Delft

Delft University of Technology

Higher-order derivatives of rigid body dynamics with application to the dynamic balance of spatial linkages

de Jong, J. J.; Müller, A.; Herder, J. L.

DOI
10.1016/j.mechmachtheory.2020.104059

Publication date
2021

Document Version
Final published version

Published in
Mechanism and Machine Theory

Citation (APA)
de Jong, J. J., Müller, A., & Herder, J. L. (2021). Higher-order derivatives of rigid body dynamics with application to the dynamic balance of spatial linkages. *Mechanism and Machine Theory*, *155*, Article 104059. https://doi.org/10.1016/j.mechmachtheory.2020.104059

Important note
To cite this publication, please use the final published version (if applicable).
Please check the document version above.

Copyright
Other than for strictly personal use, it is not permitted to download, forward or distribute the text or part of it, without the consent of the author(s) and/or copyright holder(s), unless the work is under an open content license such as Creative Commons.

Takedown policy
Please contact us and provide details if you believe this document breaches copyrights.
We will remove access to the work immediately and investigate your claim.

This work is downloaded from Delft University of Technology.
For technical reasons the number of authors shown on this cover page is limited to a maximum of 10.

Mechanism and Machine Theory 155 (2021) 104059

Contents lists available at ScienceDirect

Mechanism and Machine Theory

journal homepage: www.elsevier.com/locate/mechmachtheory

Higher-order derivatives of rigid body dynamics with application to the dynamic balance of spatial linkages

J.J. de Jong [a,*], A. Müller [b], J.L. Herder [c]

[a] Laboratory of Precision Engineering, University of Twente, PO Box 217, AE Enschede 7500, The Netherlands
[b] Johannes Kepler University, Linz, Austria
[c] Department of Precision and Microsystems Engineering, Delft University of Technology, Mekelweg 2, 2628 CD DELFT, The Netherlands

ARTICLE INFO

Article history:
Received 3 July 2020
Revised 8 August 2020
Accepted 9 August 2020
Available online 24 August 2020

Keywords:
Dynamic balance
Higher-order derivatives
Momentum
Screw theory
Parameter-linear form
Multipole representation
Rigid body dynamics
Parallel mechanisms

ABSTRACT

Dynamic balance eliminates the fluctuating reaction forces and moments induced by high-speed robots that would otherwise cause undesired base vibrations, noise and accuracy loss. Many balancing procedures, such as the addition of counter-rotating inertia wheels, increase the complexity and motor torques. There exist, however, a small set of closed-loop linkages that can be balanced by a specific design of the links' mass distribution, potentially leading to simpler and cost-effective solutions. Yet, the intricacy of the balance conditions hinder the extension of this set of linkages. Namely, these conditions contain complex closed-form kinematic models to express them in minimal coordinates. This paper presents an alternative approach by satisfying all higher-order derivatives of the balance conditions, thus avoiding finite closed-form kinematic models while providing a full solution for arbitrary linkages. The resulting dynamic balance conditions are linear in the inertia parameters such that a null space operation, either numeric or symbolic, yield the full design space. The concept of inertia transfer provides a graphical interpretation to retain intuition. A novel dynamically balanced 3-*RSR* spatially moving mechanism is presented together with known examples to illustrate the method.

© 2020 The Authors. Published by Elsevier Ltd.
This is an open access article under the CC BY license
(http://creativecommons.org/licenses/by/4.0/)

1. Introduction

Fluctuating reaction forces and moments generated by fast moving robots cause unwanted base vibrations and accuracy loss at the end-effector [1]. These shaking forces and moments may be reduced or even eliminated by a specific design of the robot's structure and inertia parameters [2]. Such mechanisms, that emit neither shaking forces nor shaking moments, are termed dynamically balanced, or force-balanced when only the shaking forces are zero. We distinguish three major approaches to design mechanisms with this feature. Firstly, one may add *supplementary counter-mechanisms* to a given mechanism, such as counter-rotating wheels [3,4] or idler loops [5–7]. Secondly, various *synthesis methods* combine and recombine elementary dynamically balanced modules such as four-bar linkages [8,9] or pantograph-like structures [10–12] into force balanced or dynamically balanced mechanisms with more degrees of freedom (DOFs). Thirdly, such an elementary module itself is obtained for the *analysis* of its dynamic balance conditions. By inspecting the equations that describe its motion and

* Corresponding author.
E-mail address: j.j.dejong@utwente.nl (J.J. de Jong).

https://doi.org/10.1016/j.mechmachtheory.2020.104059
0094-114X/© 2020 The Authors. Published by Elsevier Ltd. This is an open access article under the CC BY license
(http://creativecommons.org/licenses/by/4.0/)

dynamics, a range of inertia parameters, i.e. masses, centres of mass (COMs), and moments of inertia (MOIs) may be found that balance this specific mechanism [8,13,14].

For the viability of dynamic balance, it is essential to find simple and low-weight mechanisms that still fulfil the desired kinematic task. In this view, the addition of counter-mechanisms seems undesirable since it will increases the mass, complexity and the required motor torque. The synthesis approaches, on the other hand, have proven to be versatile for force balance, yet, incomplete for full dynamic balance [15]. In order to expand the scope of dynamic balance and to enable new synthesis methods, the focus of this paper lies in the improvement of the third approach, i.e. the generalization and the automation of the analysis approach.

The necessary and sufficient dynamic balance conditions are a constant linear and angular momentum, as their derivatives, the shaking forces and moments, then will be zero [16]. In practice, when the system is initially at rest, a zero linear and angular momentum suffices. A set of inertia parameters that satisfy these conditions is said to be a dynamically balanced solution, whereas the full description of all solutions is termed the design space of dynamically balanced inertia parameters, or design space for sake of brevity. It should be noted that open-chain linkages cannot be dynamically balanced without additional counter-mechanisms as they require zero or negative moments of inertia [4]. Closed-chain linkages, on the other hand, can in some cases by dynamically balanced by a suitable choice of inertia parameters. However, obtaining the complete design space for these linkages is not trivial as the dynamic balance conditions are to be expressed in minimal coordinates [17]. This involves kinematic loop-closure models, which may be intricate, even for relatively simple linkages [8], or unavailable in closed-form for more complex mechanisms [18]. The lack of symbolic transparency and closed-form description renders the process of solving the balance conditions an arduous task.

This complexity of the balance conditions is partly overcome by the Linear Independent Vector Method [19] and derived methods [20–22] and the Inertia Flow Method [23]. These methods eliminate only a subset of dependent coordinates, leading to simpler balancing conditions while still yielding the complete design space in general. However, in special kinematic cases, such as parallelograms, these incomplete kinematic models lead to spurious force or moment balance conditions and therefore to an incomplete description of the design space [17]. Such special kinematic cases are of particular interest for dynamic balance as they permit more solutions than the general case. For instance, Ricard and Gosselin [8] showed that the kite-type and antiparallogram-type of the planar 4*R* four-bar linkage may be fully dynamically balanced by a specific mass distribution. This in contrast to the general four-bar linkage that does require additional counter-rotating measures.

To prove the work of [8] formally, Moore et al[24]. factorized the balance conditions and loop-closure equations by means of toric geometry and Laurent polynomials. Subsequently they showed through a similar algebraic approach that the spherical four-bar linkage cannot be dynamically balanced without additional structures [25]. Currently, these algebraic methods still require a tailored inspection per mechanism and are yet to be extended to multi-DOF mechanisms. An alternative method to deal with the kinematic complexity of the loop-closure equations was adopted in [26]. There, screw theory was applied to find instantaneous dynamic balance, yielding a single pose in which mechanism accelerations will not induce shaking forces and moments. Since outside this pose the balance quality is not guaranteed, this method yields and solves only the necessary but not sufficient conditions for dynamic balance.

To summarize; in literature several systematic analysis methods were presented that solve the dynamic balance conditions for given linkages. Yet, no method yields the complete dynamically balanced design space of arbitrary linkages without a tailored manipulation of the loop-closure equations. Such a method is desired to advance our understanding of dynamic balance and to find new, simple and lightweight balance solutions.

In this paper, this long-standing problem is tackled by extending the instantaneous approach of [26] over the complete workspace by including and solving a sufficient number of higher-order derivatives of the dynamic balance conditions. The higher-order kinematic and dynamic models are readily available through recursive application of the implicit function theorem [27], thus avoiding the use of closed-form kinematic models. This method leads to the necessary and sufficient dynamic balance conditions, and an automatic and complete characterization of all dynamically balanced designs of any given non-singular mechanism consisting of lower kinematic pairs. To that end, this paper for the first time presents an algorithm to compute the derivatives of the bodies' mass matrices and momentum equations in open- and closed-loop linkages up to arbitrary order.

This paper starts with a synopsis of the method to guide the reader through the following sections (*Section 2*). Thereafter the higher-order derivatives of kinematics is outlined (*Section 3*), followed by a recapitulation of the rigid body dynamics in the screw theory framework (*Section 4*). This leads to a recursive algorithm that yields the higher-order derivatives of the linear and angular momentum equations (the dynamic balancing conditions) of open and closed-chain linkages (*Section 5*). The resulting higher-order momentum equations are then recast into the parameter-linear form [28,29] to provide dynamic balance conditions that are linear in the inertia parameters and solvable by null space algorithms (*Section 6*). General null space algorithms, i.e. singular value decomposition or Gaussian elimination, yield a complete description of all dynamically balanced mass distributions. This description however, is strongly mixed in the inertia parameters, causing a loss of interpretation and design intuition. Therefore, an alternative, meaningful description of the design space of open-chain and closed-chain linkages is presented (*Section 7*). This description is derived from the concept of *inertia transfer* and the *multipole representation of the inertia parameters*, as used in the parameter identification of robots [30]. This interpretation, here termed the multipole-rod representation, is shown to aid the feasibility study of dynamic balanced linkages. It should be noted that open chains receive quite some attention in this work. Although they cannot be dynamically balanced themselves, they provide insight into the solution space of closed-loop linkages. More specifically, it will be shown that a large

portion of the design space of a closed-loop linkage is build up from the open-chain equivalents into which the linkage may be decomposed. Case studies of a 6-DOF serial robot, a 4*R* planar four-bar linkage, and a 3-*RSR* mechanism illustrate the higher-order dynamic balance method (*Section 8*). This results in a novel 3-*RSR* mechanism design that is dynamically balanced for the 2-DOF that lie on three planes of mirror symmetry. Refer to Table A.1 for a list of symbols used in this paper.

2. Synopsis of the higher-order dynamic balance method

Ground-based open-chain linkages are dynamically balanced if the momentum $\boldsymbol{h}$ is zero for all n_b joint coordinates $\boldsymbol{q}$ and all joint velocities $\dot{\boldsymbol{q}}$. Note that this $\boldsymbol{h}$ is a combination of the linear and angular momentum and thus a 6-dimensional vector. Since the momentum must be zero for all joint velocities and since these joint velocities are linear in the momentum we obtain the following balancing condition

$$\bar{\boldsymbol{h}}(\boldsymbol{q}, \bar{\boldsymbol{z}}) \equiv \boldsymbol{0} \tag{1}$$

in which $\bar{\boldsymbol{h}} = \{\partial/\partial\dot{q}_1(\boldsymbol{h}), \ldots, \partial/\partial\dot{q}_{n_\mathrm{b}}(\boldsymbol{h})\}$ denote the collection of the basis vectors of $\boldsymbol{h}$ with respect to $\dot{\boldsymbol{q}}$. $\bar{\boldsymbol{z}}$ denotes the collection of the inertia parameters of the linkage, i.e. masses, centres of mass, and moments of inertia. The aim of this paper now lies in the derivation of the complete set of inertia parameters $\bar{\boldsymbol{z}}$ that guarantee dynamic balance for any given open- or closed-chain linkage.

For closed-loop linkages the joint coordinates $\boldsymbol{q}$ are no longer independent since a set of loop closure constraint equations hold for all motion

$$f(\boldsymbol{q}) \equiv \boldsymbol{0} \tag{2}$$

This leads to dependencies in $\boldsymbol{q}$ and $\dot{\boldsymbol{q}}$, and consequently, in a reduced set of balancing conditions. Conventionally, this dependency would be incorporated into Eq. 1 by selecting a set of minimal coordinates $\boldsymbol{u}$ and solving Eq. 2 for the dependent coordinates $\boldsymbol{q} = c(\boldsymbol{u})$. However, this approach is not always applicable as there is in general no closed form solution to the loop-closure equation, i.e. c is not always known explicitly. Furthermore, if the solution is found nevertheless, it is typically a set of involved equations that are hard to use in the balancing procedure.

In this paper we take a different, Taylor-based approach. It relies on three features. Firstly we leverage the fact that, although c might not be available in closed form, its higher-order derivatives $\mathrm{D}^k_{\boldsymbol{u}}(c)$ are available in the reference configuration $\boldsymbol{u}_0$ through a recursive application of the implicit function theorem ([27] and recapitulated in Section 3). The resulting higher-order derivatives enable a Taylor expansion of the dynamic balance conditions such that with a slight abuse of notation these read

$$\bar{\boldsymbol{h}}(\boldsymbol{u}, \bar{\boldsymbol{z}}) = \bar{\boldsymbol{h}}(\boldsymbol{u}_0, \bar{\boldsymbol{z}}) + \mathrm{D}_{\boldsymbol{u}}\big(\bar{\boldsymbol{h}}(\boldsymbol{u}_0, \bar{\boldsymbol{z}})\big)(\boldsymbol{u} - \boldsymbol{u}_0) + \frac{1}{2!}\mathrm{D}^2_{\boldsymbol{u}}\big(\bar{\boldsymbol{h}}(\boldsymbol{u}_0, \bar{\boldsymbol{z}})\big)(\boldsymbol{u} - \boldsymbol{u}_0)^2 + \cdots = \sum_{k=0}^{\infty} \frac{1}{k!}\mathrm{D}^k_{\boldsymbol{u}}\big(\bar{\boldsymbol{h}}(\boldsymbol{u}_0, \bar{\boldsymbol{z}})\big)(\boldsymbol{u} - \boldsymbol{u}_0)^k \equiv \boldsymbol{0} \tag{3}$$

As this must hold for all motion $\boldsymbol{u}$, all Taylor coefficients (the higher partial derivatives $\mathrm{D}^k_{\boldsymbol{u}}(\bar{\boldsymbol{h}})$) are required to be zero for dynamic balance. Since $\boldsymbol{h}$ and f are analytic functions in a non-singular configuration, we obtain the following necessary and sufficient conditions

$$\mathrm{D}^k_{\boldsymbol{u}}\big(\bar{\boldsymbol{h}}(\boldsymbol{u}_0, \bar{\boldsymbol{z}})\big) \equiv \boldsymbol{0} \quad \text{for} \quad k = 0 \ldots k_{\max}. \tag{4}$$

Note that this does not require an explicit solution to the loop-closure equations (Section 5). Furthermore since the balance conditions are analytic, only a finite (but unknown) number $k_{\max}$ of partial derivatives is sufficient to ensure dynamic balance, enabling an algorithmic treatment of this problem.

The second feature is that these Taylor coefficients (Eq. 4) are linear in inertia parameters $\bar{\boldsymbol{z}}$ (Section 4). The balance conditions can therefore, with the help of the regression matrix $\boldsymbol{X}_k$, be written in the form

$$\boldsymbol{X}_k(\boldsymbol{u}_0)\bar{\boldsymbol{z}} \equiv \boldsymbol{0} \quad \text{for} \quad k = 0 \ldots k_{max} \tag{5}$$

and consecutively solved by null space algorithms (Section 6), leading to a full description of the dynamically balanced mass distributions $\bar{\boldsymbol{z}} \in \ker(\boldsymbol{X}_k)$, provided that a sufficient number of derivatives is used.

Thirdly, in this paper we present a systematic partitioning and interpretation of the resulting design space in order to retain some insight in of the design dependencies and the feasibility of the solution (Section 7). We illustrate the method on known and new examples (Section 8).

3. Kinematics

In this section the groundwork of the method is laid by describing the notation and kinematics, and by recapitulating the higher-order derivatives of kinematics.

3.1. Kinematics of open-chain and closed-chain linkages using lie group and screw theory

Screw theory is used throughout this work as it gives a concise representation of the higher-order derivatives of kinematics and dynamics. This screw theory framework interprets motion of a body as a combination of an angular velocity $\boldsymbol{\omega}$ around an axis in space, passing through point $\boldsymbol{r}_t$, and a velocity along that axis, termed the pitch λ_t

$$\boldsymbol{t} = \begin{bmatrix} \boldsymbol{\omega} \\ \boldsymbol{v} \end{bmatrix} = \begin{bmatrix} \boldsymbol{\omega} \\ \boldsymbol{r}_t \times \boldsymbol{\omega} \end{bmatrix} + \lambda_t \begin{bmatrix} \boldsymbol{0} \\ \boldsymbol{\omega} \end{bmatrix} \tag{6}$$

The twist $\boldsymbol{t}$ is a function of the angular velocity $\boldsymbol{\omega}$ and the velocity $\boldsymbol{v}$ of the body's particles that instantaneously pass through the origin of the reference frame. Two special cases exist: 1) a pure rotation, i.e. the angular velocity is orthogonal to the velocity, resulting in a zero pitch ($\lambda_t = 0$), and 2) a pure translation, when the angular velocity is zero and the pitch is infinite ($\lambda_t = \infty$).

The twist of the n_b bodies in a open chain is linearly dependent on the joint velocities $\dot{\boldsymbol{q}}$ of the joints in the chain. The twist basis vector $\boldsymbol{s}_j$ associated to each joint j is termed unit twists or instantaneous screw axis (ISA). In the current context $\boldsymbol{s}_j$ is always taken in the reference configuration $\boldsymbol{q}_0$. The joints in a single chain are numbered 1 to n_b, from the base to the end-effector. Therefore, the Jacobian $\boldsymbol{J}_i$ of body i is formed by the ISAs lower in the chain

$$\boldsymbol{t}_i = \boldsymbol{J}_i \dot{\boldsymbol{q}} = \begin{bmatrix} \boldsymbol{s}_1 \cdots \boldsymbol{s}_i \boldsymbol{0} \end{bmatrix} \dot{\boldsymbol{q}}, \boldsymbol{s} = \begin{bmatrix} \boldsymbol{n} \\ \boldsymbol{r}_s \times \boldsymbol{n} \end{bmatrix} + \lambda_\mathrm{s} \begin{bmatrix} \boldsymbol{0} \\ \boldsymbol{n} \end{bmatrix}, \boldsymbol{s}_\infty = \begin{bmatrix} \boldsymbol{0} \\ \boldsymbol{n} \end{bmatrix} \tag{7}$$

These ISA are pure geometric quantities that solely dependent on the joint location $\boldsymbol{r}_\mathrm{s}$, the orientation of the joint, encoded by unit vector $\boldsymbol{n}$, and the pitch of the joint λ_s. In this case we treat the three single DOF lower kinematic pairs: revolute R, helical H, or prismatic P. For an R-joint the pitch is zero $\lambda_s = 0$, while for a P-joint the pitch is infinite $\lambda_s = \infty$, resulting in a limit case $\boldsymbol{s}_\infty$ and is therefore treated separately. Multi DOF joints, such as ball-socket joints, are treated as instantaneously identical to a set of serially connected single DOF joints.

In closed-chain linkages, the body twists are restricted by a set of loop closure conditions f. The resulting twists may be found by regarding each loop as a connection of multiple open chains. A single loop for example is opened by cutting an arbitrary body, resulting in two open chains of which the last 'virtual' bodies have the same twists. These loop-closure conditions constrain the twists of the bodies, as encoded by matrix $\boldsymbol{K}$. By selecting an independent set of n_d input coordinates $\boldsymbol{u}$, this system is solved and all dependent joint velocities determined

$$\mathrm{D}_{\boldsymbol{q}}(f)\dot{\boldsymbol{q}} = \boldsymbol{K}\bar{\boldsymbol{J}}\dot{\boldsymbol{q}} \equiv \boldsymbol{0}, \dot{\boldsymbol{q}} \in \ker(\boldsymbol{K}\bar{\boldsymbol{J}}), \dot{\boldsymbol{q}} = \boldsymbol{C}\dot{\boldsymbol{u}} \tag{8}$$

The linkage Jacobian $\bar{\boldsymbol{J}}^\top = [\boldsymbol{J}_1^\top \cdots \boldsymbol{J}_{n_\mathrm{b}}^\top]$ is the collection of all n_b body Jacobians. The $n_\mathrm{b} \times n_\mathrm{d}$ $\boldsymbol{C}$-matrix denotes the first-order solution to the loop-closure equations.

To express finite motion, a reference frame ψ_i is associated to each body i. A homogeneous transformation matrix $\boldsymbol{H}_i$, consisting of a rotation matrix $\boldsymbol{R}_i$ and a translation vector $\boldsymbol{o}_i$, express a point $\boldsymbol{a}$ from a body-fixed frame into the inertial frame of reference $\boldsymbol{a}^0 = \boldsymbol{H}_i \boldsymbol{a}^i$. In this convention the $\boldsymbol{a}^i$ vector consist of four values; 3 Cartesian coordinates and a 1. The superscripts denote the frames of expression of the vector. These transformation matrices relate again to the ISAs in a open chain through a product of matrix exponentials, leading to the general forward kinematics of open-chain linkages [31]

$$\boldsymbol{H}_i = \prod_{j=1}^{i} \exp(q_j \left[\boldsymbol{s}_j \times\right]), \boldsymbol{H} = \begin{bmatrix} \boldsymbol{R} & \boldsymbol{o}\boldsymbol{0} \\ \boldsymbol{0} & 1 \end{bmatrix}, \left[\boldsymbol{s}\times\right] = \begin{bmatrix} \left[\boldsymbol{n}\times\right] & \boldsymbol{r}_s \times \boldsymbol{n} + \lambda_s \boldsymbol{n}\boldsymbol{0} \\ \boldsymbol{0} & 0 \end{bmatrix} \tag{9}$$

in which $\exp(q_j \left[\boldsymbol{s}_j \times\right])$ denotes the matrix exponential of the 4×4 matrix of the ISA in the reference (initial) configuration ($\boldsymbol{q} = \boldsymbol{q}_0 = \boldsymbol{0}$), and $\left[\boldsymbol{n}\times\right]$ the 3×3 skew symmetric matrix of $\boldsymbol{n}$.

The ISA are expressed in another coordinate frame by the adjoint transformation matrix $\mathrm{Ad}(\boldsymbol{H})$. The ISA is expressed from the body fixed reference frame $\boldsymbol{s}_i^i$ in the inertial frame of reference $\boldsymbol{s}_i^0$ according to

$$\boldsymbol{s}_i^0 = \mathrm{Ad}(\boldsymbol{H}_i)\boldsymbol{s}_i^i, \mathrm{Ad}(\boldsymbol{H}) = \begin{bmatrix} \boldsymbol{R} & \boldsymbol{0} \\ \left[\boldsymbol{o}\times\right]\boldsymbol{R} & \boldsymbol{R} \end{bmatrix} \tag{10}$$

The time derivative of the transformation matrix relates to the body twist through the matrix form of the adjoint twist transformation, here termed adjoint twist matrix $\mathrm{ad}(\boldsymbol{t}_i)$

$$\frac{d}{dt}(\mathrm{Ad}(\boldsymbol{H}_i)) = \mathrm{ad}(\boldsymbol{t}_i)\mathrm{Ad}(\boldsymbol{H}_i), \mathrm{ad}(\boldsymbol{t}) = \begin{bmatrix} \left[\boldsymbol{\omega}\times\right] & \boldsymbol{0} \\ \left[\boldsymbol{v}\times\right] & \left[\boldsymbol{\omega}\times\right] \end{bmatrix} \tag{11}$$

3.2. Higher-order derivatives of kinematics

For parallel mechanism a closed-form solution to the kinematic loop-closure equations does not exist in general. Yet, a higher-order approximation of the motion is available by treating the closed loop as a connection of several open chains. For such a connection, the higher-order derivatives of the loop-closure equations are found and solved yielding a Taylor

approximation of finite motion [27]. In that approach, the higher-order partial derivatives of the body twists are found from the adjoint twist matrices corresponding to the ISA that are lower in the open-chain equivalent linkage [32]. Since each ISA is constant when expressed in a local body-fixed frame, all these derivatives follow from a repetitive application of Eq. 11 to Eq. 10, such that

$$\mathrm{D}_{\boldsymbol{q}}^{\boldsymbol{\alpha}}(\boldsymbol{s}_i) = \prod_{j=1}^{i-1} \mathrm{ad}\left(\boldsymbol{s}_j\right)^{\alpha_j} \boldsymbol{s}_i \tag{12}$$

In here $\mathrm{D}_{\boldsymbol{q}}^{\boldsymbol{\alpha}}(\boldsymbol{A}) = \partial^k/(\partial q_1^{\alpha_1} \cdot \ldots \cdot \partial q_n^{\alpha_n})(\boldsymbol{A})$ denotes the higher-order partial derivatives with respect to the elements of $\boldsymbol{q}$. Vector $\boldsymbol{\alpha} = (\alpha_1, \ldots, \alpha_n)$ comprises the order of the derivatives corresponding to $\boldsymbol{q}$, running from the base to the end-effector. Hence we assume an ordered sequence, i.e. α_i corresponds to the joint q_i. The $k = \alpha_1 + \ldots + \alpha_n = |\boldsymbol{\alpha}|$ is the total order, see Appendix A. The joints higher in the chain have no contribution to the motion of the lower joints, such that this derivative (Eq. 12) is set to zero, i.e. if $\alpha_j \neq 0$ for $j \geq i$. By this, all the higher-order partial derivatives of the body Jacobians $\mathrm{D}_{\boldsymbol{q}}^{\boldsymbol{\alpha}}(\boldsymbol{J}_i)$ are available.

This procedure is used for the solution of the higher-order closed-loop constraints [27] by recasting it into the matrix derivative framework of Vetter for bookkeeping [33] and Appendix A. In this notation the collection of all first-order partial derivatives of matrix $\boldsymbol{A} = [\boldsymbol{a}_1 \quad \cdots \quad \boldsymbol{a}_m]$ are sorted according to[1]

$$\mathrm{D}_{\boldsymbol{q}}(\boldsymbol{A}) = \left[\mathrm{D}_{\boldsymbol{q}}(\boldsymbol{a}_1) \quad \cdots \quad \mathrm{D}_{\boldsymbol{q}}(\boldsymbol{a}_m)\right], \mathrm{D}_{\boldsymbol{q}}(\boldsymbol{a}_i) = \left[\partial/\partial q_1(\boldsymbol{a}_i) \quad \cdots \quad \partial/\partial q_n(\boldsymbol{a}_i)\right] \tag{13}$$

With this, the derivatives of the loop-closure solution $\mathrm{D}_{\boldsymbol{u}}(\boldsymbol{C})$ are found through application of the chain rule and product rule (Appendix A) to Eq. 8. The collection of second-order loop-closure constraints read

$$\mathrm{D}_{\boldsymbol{q}}\left(\boldsymbol{K}\bar{\boldsymbol{J}}\right)(\boldsymbol{C}\otimes\boldsymbol{C}) + \boldsymbol{K}\bar{\boldsymbol{J}}\mathrm{D}_{\boldsymbol{u}}(\boldsymbol{C}) \equiv \boldsymbol{0} \tag{14}$$

In here $\boldsymbol{A}\otimes\boldsymbol{B}$ denotes the Kronecker product of two matrices (Appendix A). From this equation $\mathrm{D}_{\boldsymbol{u}}(\boldsymbol{C})$ is determined. A recursive application leads to the k-th order constraints

$$\mathrm{D}_{\boldsymbol{u}}^k\left(\boldsymbol{K}\bar{\boldsymbol{J}}\boldsymbol{C}\right) = \sum_{i=1}^{n_b} \left[\mathrm{D}_{\boldsymbol{q}}^k\left(\boldsymbol{K}\bar{\boldsymbol{J}}\right) \quad \cdots \quad \boldsymbol{K}\bar{\boldsymbol{J}}\right]\bar{\boldsymbol{C}}_k \equiv \boldsymbol{0}, (\bar{\boldsymbol{C}}_k)^\top = \left[(\boldsymbol{C}^{\otimes k})^\top \quad \cdots \quad \mathrm{D}_{\boldsymbol{u}}^k(\boldsymbol{C})^\top\right] \tag{15}$$

from which $\mathrm{D}_{\boldsymbol{u}}^k(\boldsymbol{C})$ may be solved through the algorithm presented in [27]. The Kronecker power is denoted by a $\otimes k$ superscript. The exact composition of the $\bar{\boldsymbol{C}}_k$ collection matrix is found through repetitive application of the chain and product rules, but is omitted here due to space limitation.

4. Rigid body dynamics

The rigid body dynamics of spatially moving objects and mechanisms is concisely written with the use of screw theory [34,35]. This section briefly introduces the use of screw and Lie group theory in rigid body dynamics, followed by the presentation of the multipole-rod representation of the inertia parameters as used in the interpretation of the dynamically balanced solution later on.

4.1. Momentum wrench and mass matrix

The momentum of a body is the product of the body's spatial mass matrix $\boldsymbol{M}$ and the twist $\boldsymbol{t}$ associated to it. The momentum is a co-screw or a wrench-like entity and therefore termed momentum wrench hereafter

$$\boldsymbol{h} = \begin{bmatrix} \boldsymbol{\xi} \\ \boldsymbol{p} \end{bmatrix} = \boldsymbol{M}\boldsymbol{t}. \tag{16}$$

The mass matrix of a body is formed by the integral over the body volume

$$\boldsymbol{M} = \int_V \begin{bmatrix} -[\boldsymbol{r}\times]^2 & [\boldsymbol{r}\times] \\ -[\boldsymbol{r}\times] & \boldsymbol{I}_3 \end{bmatrix} \mathrm{d}m = \begin{bmatrix} \boldsymbol{E} & [m\boldsymbol{c}\times] \\ -[m\boldsymbol{c}\times] & m\boldsymbol{I}_3 \end{bmatrix}. \tag{17}$$

This gives rise to the classical description with a mass m, a centre of mass $\boldsymbol{c}$ and inertia matrix $\boldsymbol{E}$ with respect to the inertial frame of reference. The inertia matrix $\boldsymbol{E}$ contains 3 inertia moments and 3 products of inertia, respectively on its diagonal $\boldsymbol{e}_\mathrm{d}^\top = [e_1 \quad e_2 \quad e_3]$ and its off diagonal $\boldsymbol{e}_\mathrm{o}^\top = [e_4 \quad e_5 \quad e_6]$. The matrix $\boldsymbol{I}_3$ denotes a 3×3 identity matrix. Due to the frame invariance of kinetic energy $K = 1/2\boldsymbol{t}^\top\boldsymbol{M}\boldsymbol{t}$, the mass matrix transforms with an adjoint transformation matrix on the right and its transposed on the left. By choosing a frame that is located at the centre of mass and aligned with the principal axis

[1] Please note the two distinct uses of the differentiation operator. When the superscript is a vector, i.e. $\mathrm{D}_{\boldsymbol{q}}^{\boldsymbol{\alpha}}$, it denotes a repeated partial derivatives, but when the superscript is a scalar, i.e. $\mathrm{D}_{\boldsymbol{q}}^k$, it is a collection of partial derivatives of order k (Appendix A).

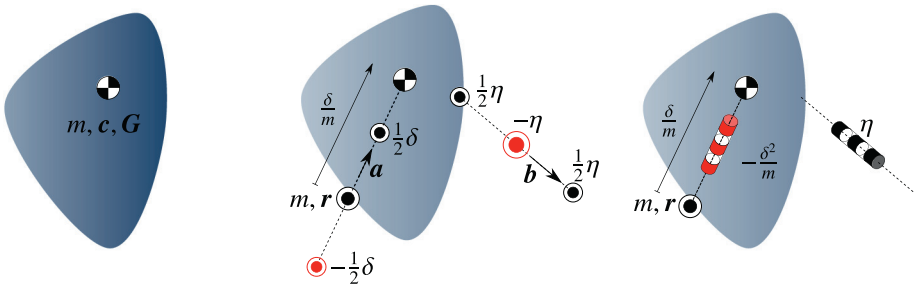

(a) Conventional (b) Multipole (c) Multipole-rod

Fig. 1. Three representations of the inertia parameters of a body. (a) The conventional representation with a mass m, a centre of mass $\boldsymbol{c}$ and an inertia matrix $\boldsymbol{G}$ around $\boldsymbol{c}$. (b) The multipole representation [30] with parameters that are linear in the mass matrix; a monopole m at $\boldsymbol{r}$, a dipole δ in the direction $\boldsymbol{a}$, and a quadripole η in the direction of $\boldsymbol{b}$. One monopole, three dipoles and six quadripoles are sufficient to describe arbitrary bodies. (c) The multipole-rod representation reduces the number of graphical elements by interpreting the quadripole as an infinitely long, slender rod, termed 'pure-inertia rod' and depicted as a striped bar. The monopole is termed 'point mass', whereas the dipole is treated as a 'displacement' of the point mass with negative pure-inertia rod in the same direction.

of inertia, any mass matrix can be diagonalized. The corresponding transformation matrix from this principal axes frame to the current frame is $\mathrm{Ad}(\boldsymbol{H}_\mathrm{p})$. This gives rise to three principal MOIs g_1, g_2, and g_3

$$\boldsymbol{M} = \mathrm{Ad}(\boldsymbol{H}_\mathrm{p})^{-\top}\,\mathrm{diag}(g_1, g_2, g_3, m, m, m)\mathrm{Ad}(\boldsymbol{H}_\mathrm{p})^{-1}. \tag{18}$$

In this body-fixed frame, the mass matrix is constant, i.e. $\dot{m}$ and $\dot{g}_i = 0$, due to the rigid body assumption. Since the mass matrix is formed by a collection of positive mass particles, the mass matrix itself is symmetric positive definite, leading to 7 inequality conditions on the mass and the principal MOIs

$$m > 0, g_i > 0, g_i + g_j > g_k \tag{19}$$

4.2. Momentum wrench basis

Similar to the twist basis, we define a linkage's momentum basis that spans all possible momentum wrenches at a given pose. The basis vectors, termed the instantaneous momentum wrenches (IMW) and denoted with $\hat{\boldsymbol{h}}_i$, are the momentum wrenches generated by unit actuation of each joint. The total momentum wrench of a open chain is therefore given by

$$\boldsymbol{h} = \sum \boldsymbol{M}_i \boldsymbol{t}_i = \bar{\boldsymbol{M}}\bar{\boldsymbol{J}}\dot{\boldsymbol{q}} = \begin{bmatrix}\hat{\boldsymbol{h}}_1 & \cdots & \hat{\boldsymbol{h}}_n\end{bmatrix}\dot{\boldsymbol{q}} \equiv 0, \hat{\boldsymbol{h}}_i = \sum_{j=i}^{n_\mathrm{b}} \boldsymbol{M}_j \boldsymbol{s}_i \equiv 0 \tag{20}$$

In here $\bar{\boldsymbol{M}} = [\boldsymbol{M}_1 \quad \cdots \quad \boldsymbol{M}_n]$ denotes the collection of all mass matrices in the chain. For dynamic balance all the IMWs must be zero for arbitrary motion. For closed-chain linkages the momentum wrench basis is computed by applying the first order loop-closure solution $\boldsymbol{C}$

$$\boldsymbol{h} = \bar{\boldsymbol{M}}\bar{\boldsymbol{J}}\boldsymbol{C}\dot{\boldsymbol{u}} \equiv \boldsymbol{0}. \tag{21}$$

4.3. Multipole-rod interpretation of the mass matrix

In the current dynamic balancing procedure we will use the fact that the balancing conditions are linear in the elements of the mass matrix such that they can be solved through a set of linear operations. The conventional mass matrix parametrisation, consisting of masses m, COMs $\boldsymbol{c}$ and principal MOIs $\boldsymbol{g}$, is not suitable for the interpretation of the resulting design space, since it is not linear in the elements of the mass matrix. Therefore we will use a slight adaptation of the multipole concept of Ros et al[30]., termed the multipole-rod representation (Fig. 1). This interpretation relies on the fact that a mass matrix can be decomposed into three primitive elements; 1) a single *point mass* at $\boldsymbol{r}$, denoted with a subscript m, 2) a *displacement* of the point mass in the direction of a unit vector $\boldsymbol{a}$ combined with a pure-inertia rod of opposite magnitude, denoted with a subscript δ, and 3) a *pure-inertia rod* in the direction of a unit vector $\boldsymbol{b}$, denoted with a subscript η. These pure-inertia rods are interpreted as infinitely long slender rods in the direction of their unit vector. Their mass is assumed zero such that only the rotational velocity component in a perpendicular direction generates angular momentum. A rotation around their longitudinal axis generates no angular momentum. The sole difference with the method of [30] is the graphical representation. This reduces the larger number of point masses (poles), which otherwise might congest the figures.

Now, any mass matrix can be represented by choice of 10 of these primitive elements, one point mass, three displacements, and six pure-inertia rods, as long as the unit vectors $\boldsymbol{a}_i$ and $\boldsymbol{b}_i$ are unique

$$\boldsymbol{M} = m\boldsymbol{M}_m(\boldsymbol{r}) + \sum_{i=1\cdots3} \delta_i \boldsymbol{M}_\delta(\boldsymbol{a}_i, \boldsymbol{r}) + \sum_{i=1\cdots6} \eta_i \boldsymbol{M}_\eta(\boldsymbol{b}_i). \tag{22}$$

The mass, the moment of mass, and the moment of inertia of these elements are given by

$$m_m = 1,\ (m\boldsymbol{c})_m = \boldsymbol{r},\ \boldsymbol{E}_m = -\left[\boldsymbol{r}\times\right]^2,\ m_\delta = 0,\ (m\boldsymbol{c})_\delta = \boldsymbol{a},\ \boldsymbol{E}_\delta = 1/2\left[\boldsymbol{r}-\boldsymbol{a}\times\right]^2 - 1/2\left[\boldsymbol{r}+\boldsymbol{a}\times\right]^2,$$
$$m_\eta = 0,\ (m\boldsymbol{c})_\eta = \boldsymbol{0},\ \boldsymbol{E}_\eta = -\left[\boldsymbol{b}\times\right]^2. \tag{23}$$

For the planar case, this representation requires one point mass, two displacements and one pure-inertia rod, of which the elements reduce to

$$m_m = 1,\ (m\boldsymbol{c})_m = \boldsymbol{r},\ e_m = \|\boldsymbol{r}\|^2,\ m_\delta = 0,\ (m\boldsymbol{c})_\delta = \boldsymbol{a},\ e_\delta = 2\boldsymbol{a}^\top\boldsymbol{r},\ m_\eta = 0,\ (m\boldsymbol{c})_\eta = \boldsymbol{0},\ e_\eta = 1. \tag{24}$$

For feasibility of each body, they must consist of at least one positive point mass, and three non-coplanar positive pure-inertia rods (Eq. 19), since two pure-inertia rods represent an infinitely flat object. A negative pure-inertia rod requires at least 3 arbitrarily oriented positive pure-inertia rods (or two positive coplanar pure-inertia rods) of sufficient magnitude to represent a feasible body. A closed-form feasibility description of an arbitrary collection of these elements can be found through eigendecomposition of the resulting mass matrix, but lies outside the scope of this paper.

5. Higher-order derivatives of the momentum equations and of the dynamic balance conditions

The previously presented higher-order analysis of the kinematics is extended to rigid body dynamics in this section. The aim is to find and solve the necessary and sufficient dynamic balance conditions of arbitrary linkages without invoking the closed-form solution to the loop-closure equations. For dynamic balancing purposes this study is confined to the change of rigid body momentum. Other effects such as gravity, elasticity, or external forces are not taken into account. The dynamic balance conditions are obtained from the partial derivatives of the mass matrices and momentum equations of open-chain linkages, which are extended thereafter to closed-chain linkages by including the higher-order derivatives of the loop-closure solution. It should be noted that although open-chain linkages cannot be dynamically balanced without additional counter-mechanisms, their description is important for dynamic balance since closed-loop linkages can be regarded as connected open chains.

5.1. Derivatives of the mass matrix in a open chain

The mass matrix of a body i in a open chain depends on the pose of the joints that are lower in the kinematic chain according to Eq. 9 and Eq. 18. Therefore, its partial derivative with respect to a joint j, lower in the chain ($j \leq i$), is found by applying Eq. 11 to Eq. 18

$$\frac{\partial}{\partial q_j}(\boldsymbol{M}_i) = -\mathrm{ad}\left(\boldsymbol{s}_j\right)^\top \boldsymbol{M}_i - \boldsymbol{M}_i \mathrm{ad}\left(\boldsymbol{s}_j\right) \tag{25}$$

Here we have used the fact that the mass matrix is constant in the body-fixed frame. For all partial derivatives with respect to joints higher in the chain ($j > i$) this derivative is zero.

A second (non-zero) partial derivative is either with respect to a joint higher ($j \leq l \leq i$) or joint lower ($l \leq j \leq i$) in the chain. In the first case ($j \leq l \leq i$) the partial derivative becomes

$$\frac{\partial}{\partial q_l}\frac{\partial}{\partial q_j}(\boldsymbol{M}_i) = \mathrm{ad}\left(\boldsymbol{s}_l\right)^\top \left(\mathrm{ad}\left(\boldsymbol{s}_j\right)^\top \boldsymbol{M}_i + \boldsymbol{M}_i \mathrm{ad}\left(\boldsymbol{s}_j\right)\right) + \left(\mathrm{ad}\left(\boldsymbol{s}_j\right)^\top \boldsymbol{M}_i + \boldsymbol{M}_i \mathrm{ad}\left(\boldsymbol{s}_j\right)\right)\mathrm{ad}\left(\boldsymbol{s}_l\right). \tag{26}$$

Here the Jacobi identity $\partial/\partial q_l(\mathrm{ad}\left(\boldsymbol{s}_j\right)) = \mathrm{ad}(\mathrm{ad}\left(\boldsymbol{s}_l\right)\boldsymbol{s}_j) = \mathrm{ad}\left(\boldsymbol{s}_l\right)\mathrm{ad}\left(\boldsymbol{s}_j\right) - \mathrm{ad}\left(\boldsymbol{s}_j\right)\mathrm{ad}\left(\boldsymbol{s}_l\right)$ is used. For the second case ($l \leq j \leq i$) only the derivative of the mass matrix has to be taken into account as a higher joint does not influence a lower ISA ($\partial/\partial q_l(\mathrm{ad}\left(\boldsymbol{s}_j\right)) = 0$). This results in a similar equation as Eq. 26, with the sole difference that the indices j and l are swapped. This also follows from the symmetry of partial derivatives. This nested structure, i.e. the pre- and postmultiplication of adjoint twist matrices, is preserved for the higher orders, leading to a recursive formula for all partial derivatives of the mass matrix

$$\frac{\partial}{\partial q_j}(\mathrm{D}^{\boldsymbol{\alpha}}_{\boldsymbol{q}}(\boldsymbol{M}_i)) = -\mathrm{ad}\left(\boldsymbol{s}_j\right)^\top \mathrm{D}^{\boldsymbol{\alpha}}_{\boldsymbol{q}}(\boldsymbol{M}_i) - \mathrm{D}^{\boldsymbol{\alpha}}_{\boldsymbol{q}}(\boldsymbol{M}_i)\mathrm{ad}\left(\boldsymbol{s}_j\right) \tag{27}$$

in here j is the lowest joint to which a partial derivative is taken, i.e. $\alpha_l = 0$ for all $l < j$. In case $\alpha_l \neq 0$ for any $l > i$, this equation is set to zero.

5.2. Derivatives of the momentum wrench in a open chain

Now that the derivatives of the mass matrix up to arbitrary order are available, we consider the partial derivatives of the momentum wrench with the aim of obtaining all higher-order dynamic balance conditions. Consider the momentum wrench generated by the jth body due to unit actuation of joint i, which is lower in the chain. Two types of non-zero partial derivatives appear. Either joint l — with respect to which the derivative is taken — is below the joint i, or between

the joint i and the jth body. In the first case ($l \leq i \leq j$), the partial derivative of both the mass matrix and the ISA have to be taken into account, partially canceling out

$$\frac{\partial}{\partial q_l}\left(\boldsymbol{M}_j \boldsymbol{s}_i\right) = \frac{\partial}{\partial q_l}\left(\boldsymbol{M}_j\right)\boldsymbol{s}_i + \boldsymbol{M}_j \frac{\partial}{\partial q_l}\left(\boldsymbol{s}_i\right) = -\mathrm{ad}\left(\boldsymbol{s}_l\right)^\top \boldsymbol{M}_j \boldsymbol{s}_i. \tag{28}$$

In the second case ($i < l \leq j$), the partial derivative of the ISA vanishes $\partial / \partial q_l(\boldsymbol{s}_i) = 0$. Therefore, the partial derivative of the momentum wrench becomes

$$\frac{\partial}{\partial q_l}\left(\boldsymbol{M}_j \boldsymbol{s}_i\right) = \frac{\partial}{\partial q_l}\left(\boldsymbol{M}_j\right)\boldsymbol{s}_i = -(\mathrm{ad}\left(\boldsymbol{s}_l\right)^\top \boldsymbol{M}_j + \boldsymbol{M}_j \mathrm{ad}\left(\boldsymbol{s}_l\right))\boldsymbol{s}_i. \tag{29}$$

The higher-order partial derivatives are found similarly by making a split between the partial derivatives related to joints lower than the momentum generating ISA, and the ones related to the joints between the ISA and the body. Therefore. a second multi-index is introduced for which holds $\beta_l = \alpha_l$ for all $i < l \leq j$ and $\beta_l = 0$ for all $l \leq i$. The partial derivatives of the momentum wrench are found from Eq. 27 according to

$$\mathrm{D}_{\boldsymbol{q}}^{\boldsymbol{\alpha}}\left(\boldsymbol{M}_j \boldsymbol{s}_i\right) = \prod_{l=1}^{i} \left(-\mathrm{ad}\left(\boldsymbol{s}_l\right)^\top\right)^{\alpha_l} \mathrm{D}_{\boldsymbol{q}}^{\boldsymbol{\beta}}\left(\boldsymbol{M}_j\right)\boldsymbol{s}_i. \tag{30}$$

Again this equation is zero if $\alpha_l \neq 0$ for any $l > j$. These partial derivatives may be summed to obtain the derivatives of the total momentum of the linkage. Notice that in this equation the momentum derivatives are formulated as a sequence of matrix operations, which are linear in the mass matrix.

5.3. Derivatives of the dynamic balance conditions of a open-chain linkages

The dynamic balance conditions dictate that the momentum wrench of a linkage is zero for all motion. Therefore also all higher-order derivatives of the momentum wrench must be zero. With a large enough number of derivatives k_{max} these are not only the necessary but also the sufficient dynamic balance conditions for nonsingular linkages. In fact, here it will be shown that for open-chain linkages only derivatives up to the second order are needed ($k_{\max} \leq 2$). When these are satisfied, all the higher-order dynamic balance conditions satisfied, and the linkage is dynamically balanced for finite motion.

For zeroth-order dynamic balance, the condition (Eq. 20) imposed on each IMW is

$$\hat{\boldsymbol{h}}_i = \sum_{j=i}^{n_\mathrm{b}} \boldsymbol{M}_j \boldsymbol{s}_i = \tilde{\boldsymbol{M}}_i \boldsymbol{s}_i \equiv \boldsymbol{0}, \tilde{\boldsymbol{M}}_i = \sum_{j=i}^{n_\mathrm{b}} \boldsymbol{M}_j = \begin{bmatrix} \tilde{\boldsymbol{E}}_i & \left[\widetilde{m_i \boldsymbol{c}_i}\times\right] \\ -\left[\widetilde{m_i \boldsymbol{c}_i}\times\right] & \tilde{m}_i \boldsymbol{I}_3 \end{bmatrix} \tag{31}$$

The aggregated mass matrix $\tilde{\boldsymbol{M}}_i$ is the sum of the mass matrices belonging to bodies higher in the chain than $\boldsymbol{s}_i$. Consider now the following momentum derivatives of $\hat{\boldsymbol{h}}_j$ and $\hat{\boldsymbol{h}}_l$, involving any triplet $\boldsymbol{s}_l$, $\boldsymbol{s}_j$, and $\boldsymbol{s}_i$ of zero or finite pitch ISA, which are arranged in ascending order ($l \leq j \leq i$)

$$\frac{\partial}{\partial q_i}\left(\hat{\boldsymbol{h}}_l\right) = \frac{\partial}{\partial q_i}\left(\tilde{\boldsymbol{M}}_i\right)\boldsymbol{s}_l \equiv \boldsymbol{0}, \qquad \frac{\partial}{\partial q_i}\left(\hat{\boldsymbol{h}}_j\right) = \frac{\partial}{\partial q_i}\left(\tilde{\boldsymbol{M}}_i\right)\boldsymbol{s}_j \equiv \boldsymbol{0} \tag{32}$$

$$\frac{\partial}{\partial q_l}\frac{\partial}{\partial q_i}\left(\hat{\boldsymbol{h}}_j\right) = -\mathrm{ad}\left(\boldsymbol{s}_l\right)^\top \frac{\partial}{\partial q_i}\left(\hat{\boldsymbol{h}}_j\right) - \frac{\partial}{\partial q_i}\left(\tilde{\boldsymbol{M}}_i\right)\mathrm{ad}\left(\boldsymbol{s}_l\right)\boldsymbol{s}_j \equiv \boldsymbol{0} \tag{33}$$

Notice that these dynamic balancing conditions impose constraints on the same aggregated mass matrix $\tilde{\boldsymbol{M}}_i$ since q_i is higher in the chain than q_l and q_j such that $\partial / \partial q_i(\boldsymbol{M}_j) = 0$ for $j \leq i$. As the first-order balancing conditions (Eq. 32.b) ensure that $\partial / \partial q_i(\hat{\boldsymbol{h}}_j) = 0$, the second-order dynamic balance conditions (Eq. 33) reduce to

$$\frac{\partial}{\partial q_i}\left(\tilde{\boldsymbol{M}}_i\right)\mathrm{ad}\left(\boldsymbol{s}_l\right)\boldsymbol{s}_j \equiv \boldsymbol{0} \tag{34}$$

A recursive application shows that this extends to the higher orders, such that all balance conditions are of the form

$$\frac{\partial}{\partial q_i}\left(\tilde{\boldsymbol{M}}_i\right)\prod_{l=j}^{i}\left(\mathrm{ad}\left(\boldsymbol{s}_l\right)^\top\right)^{\alpha_l}\boldsymbol{s}_j \equiv \boldsymbol{0} \tag{35}$$

Moreover, the zeroth-order balance conditions (Eq. 31) satisfies all higher-order force balancing conditions since $\partial / \partial q_i(\tilde{\boldsymbol{M}}_i)$ is a function of the linear momentum and the mass is assumed to be constant

$$\frac{\partial}{\partial q_i}\left(\widetilde{m_i \boldsymbol{c}_i}\right) = \hat{\boldsymbol{p}}_i \equiv \boldsymbol{0}, \frac{\partial}{\partial q_i}\left(\tilde{m}_i\right) = \boldsymbol{0} \tag{36}$$

Therefore, only the following first- and second-order moment balance conditions remain:

$$\frac{\partial}{\partial q_i}\left(\tilde{\boldsymbol{E}}_i\right)\boldsymbol{n}_l \equiv \boldsymbol{0}, \frac{\partial}{\partial q_i}\left(\tilde{\boldsymbol{E}}_i\right)\boldsymbol{n}_j \equiv \boldsymbol{0}, \frac{\partial}{\partial q_i}\left(\tilde{\boldsymbol{E}}_i\right)\left[\boldsymbol{n}_l\times\right]\boldsymbol{n}_j \equiv \boldsymbol{0} \tag{37}$$

In the general case, when $\boldsymbol{n}_j \nparallel \boldsymbol{n}_l$, this imposes 9 independent constraints on the derivative of the inertia matrix, requiring $\partial/\partial q_i(\tilde{\boldsymbol{E}}_i) = \boldsymbol{0}$, thus directly satisfying all higher-order partial derivatives (Eq. 35). This shows that derivatives of a higher order than $k_{\max} = 2$ impose no new dynamic balance conditions for open-chain linkages. When, in the special case, all non-infinite pitch ISA lower in the chain are parallel, i.e. $\boldsymbol{n}_j \| \boldsymbol{n}_i$ for all $j < i$, the moment balance conditions (Eq. 37) vanish or become equivalent. Then, only three higher-order constraints are imposed on the aggregated inertia matrix $\tilde{\boldsymbol{E}}_i$. Prismatic joints (infinite pitch ISA) lower in the chain impose no higher-order moment balance conditions as their angular velocities $\boldsymbol{n}_j$ are zero.

To summarize: for open-chain linkages the zero-order force and moment balance conditions (Eq. 31) and the first- and second-order moment balance conditions (Eq. 37) are necessary and sufficient, leading to a $k_{\max} = 2$.

5.4. Derivatives of the dynamic balance conditions of closed-chain linkages

The dynamic balance conditions of closed-chain linkages dictate a zero momentum wrench (Eq. 21) for all independent velocities $\dot{\boldsymbol{u}}$. Therefore the zeroth-order balancing conditions read

$$\bar{\boldsymbol{M}}\bar{\boldsymbol{J}}\boldsymbol{C} \equiv \boldsymbol{0} \tag{38}$$

Also all higher-order partial derivatives with respect to $\boldsymbol{u}$ should be zero for dynamic balance. These conditions are found by repetitive application of the chain rule, the product rule and derivatives of the Kronecker product. Similar to Eq. 15, the first-order dynamic balancing conditions become

$$\mathrm{D}_{\boldsymbol{u}}\left(\bar{\boldsymbol{M}}\bar{\boldsymbol{J}}\boldsymbol{C}\right) = \mathrm{D}_{\boldsymbol{q}}\left(\bar{\boldsymbol{M}}\bar{\boldsymbol{J}}\right)(\boldsymbol{C}\otimes\boldsymbol{C}) + \bar{\boldsymbol{M}}\bar{\boldsymbol{J}}\mathrm{D}_{\boldsymbol{u}}(\boldsymbol{C}) \equiv \boldsymbol{0} \tag{39}$$

This generalizes to higher-orders by a repetitive application of the chain and product rules

$$\mathrm{D}^k_{\boldsymbol{u}}\left(\bar{\boldsymbol{M}}\bar{\boldsymbol{J}}\boldsymbol{C}\right) = \begin{bmatrix}\mathrm{D}^k_{\boldsymbol{q}}\left(\bar{\boldsymbol{M}}\bar{\boldsymbol{J}}\right) & \cdots & \bar{\boldsymbol{M}}\bar{\boldsymbol{J}}\end{bmatrix}\bar{\boldsymbol{C}}_k \equiv \boldsymbol{0} \tag{40}$$

From the analyticity of the momentum equations it may be deduced that there is finite $k_{\max}$ which renders these conditions not only necessary but also sufficient for the dynamic balance for closed chains in nonsingular poses. Refer to Section 9 for a discussion on the necessity and sufficiency of these conditions.

It should be noted that these higher-order dynamic balance conditions are linear in the mass matrices and can be obtained through a series of matrix multiplications and linear operations. This method is therefore able to treat symbolic or numerical input.

6. Dynamic balance solution using the parameter-linear form

Now, to solve these higher-order dynamic balance conditions, we recast Eq. 40 in the parameter-linear form [28,29] as used in the parameter identification. This enables null space procedures to extract the dynamically balanced mass distributions.

6.1. Parameter-linear form

Since the m, $m\boldsymbol{c}$ and $\boldsymbol{E}$ (Eq. 17) are linear in the momentum equation, the following parameter-linear form holds

$$\boldsymbol{h} = \boldsymbol{M}\boldsymbol{t} = \begin{bmatrix}\boldsymbol{t}*\end{bmatrix}\boldsymbol{z}, \boldsymbol{z}^\top = \begin{bmatrix} m & m\boldsymbol{c}^\top & \boldsymbol{e}_{\mathrm{d}}^\top & \boldsymbol{e}_{\mathrm{o}}^\top \end{bmatrix} \tag{41}$$

in which the $\boldsymbol{z}$-vector is formed by the inertia parameters of the body. The twist dependent 'regression' matrix is given by

$$\begin{bmatrix}\boldsymbol{t}*\end{bmatrix} = \begin{bmatrix} \boldsymbol{0} & -\begin{bmatrix}\boldsymbol{v}\times\end{bmatrix} & \mathrm{diag}(\boldsymbol{\omega}) & \begin{bmatrix}\boldsymbol{\omega}*\end{bmatrix} \\ \boldsymbol{v} & \begin{bmatrix}\boldsymbol{\omega}\times\end{bmatrix} & \boldsymbol{0} & \boldsymbol{0} \end{bmatrix}, \begin{bmatrix}\boldsymbol{\omega}*\end{bmatrix} = \begin{bmatrix} \omega_5 & \omega_6 & 0 \\ \omega_4 & 0 & \omega_6 \\ 0 & \omega_4 & \omega_5 \end{bmatrix}. \tag{42}$$

Notice that the ordering of the inertia parameter slightly differs from [29]. The parameter-linear form of the momentum basis of a open-chain linkages is directly computed from Eq. 20

$$\bar{\boldsymbol{h}} = \mathrm{vec}(\bar{\boldsymbol{M}}\bar{\boldsymbol{J}}) = \begin{bmatrix}\hat{\boldsymbol{h}}_1 \\ \vdots \\ \hat{\boldsymbol{h}}_n\end{bmatrix} = \begin{bmatrix}\begin{bmatrix}\boldsymbol{s}_1*\end{bmatrix} & \cdots & \begin{bmatrix}\boldsymbol{s}_1*\end{bmatrix} \\ \vdots & \ddots & \vdots \\ 0 & \cdots & \begin{bmatrix}\boldsymbol{s}_n*\end{bmatrix}\end{bmatrix}\begin{bmatrix}\boldsymbol{z}_1 \\ \vdots \\ \boldsymbol{z}_n\end{bmatrix} = \boldsymbol{W}\bar{\boldsymbol{z}} \tag{43}$$

in here $\bar{\boldsymbol{h}}$ and $\bar{\boldsymbol{z}}$ denote the concatenation of all IWM and all inertia parameters in the chain, respectively.

To obtain the parameter-linear form of closed-chain linkages, the vectorization of matrix products (Appendix A) is applied to Eq. 38

$$\bar{\boldsymbol{h}} = \mathrm{vec}(\bar{\boldsymbol{M}}\bar{\boldsymbol{J}}\boldsymbol{C}) = (\boldsymbol{C}^\top\otimes\boldsymbol{I}_6)\boldsymbol{W}\bar{\boldsymbol{z}} = \boldsymbol{X}\bar{\boldsymbol{z}} \tag{44}$$

where $\boldsymbol{I}_6$ is a 6×6 identity matrix.

6.2. Higher-order dynamic balance conditions in the parameter-linear form

The parameter-linear form also applies to higher-order derivatives of the balance conditions as they are formed through a sequence of matrix operations that are linear the inertia parameters. The higher-order open chain regression matrices $\boldsymbol{W}_k$ can be found accordingly, i.e. by the application of Eq. 41 to Eq. 27 and Eq. 30, resulting in the following condition

$$\mathrm{vec}\left(\mathrm{D}_{\boldsymbol{q}}^{k}(\bar{\boldsymbol{h}})\right) = \boldsymbol{W}_k \bar{\boldsymbol{z}} \equiv \boldsymbol{0} \tag{45}$$

For closed chains the parameter-linear form is found by applying the matrix vectorization to Eq. 40, such that

$$\mathrm{vec}\left(\mathrm{D}_{\boldsymbol{q}}^{k}(\bar{\boldsymbol{h}})\right) = (\bar{\boldsymbol{C}}_k^{\top} \otimes \boldsymbol{I}_6)\bar{\boldsymbol{W}}_k \bar{\boldsymbol{z}} = \boldsymbol{X}_k \bar{\boldsymbol{z}} \equiv \boldsymbol{0} \tag{46}$$

in which $\bar{\boldsymbol{W}}_k^{\top} = \begin{bmatrix}\boldsymbol{W}_1^{\top} & \cdots & \boldsymbol{W}_k^{\top}\end{bmatrix}$. Now we have arrived at the parameter-linear form of the higher-order derivatives of the momentum equations of open- and closed-chain linkages. It should be observed that all these steps solely rely on matrix operations suitable for algorithmic treatment.

6.3. Solving the dynamic balance condition

Dynamic balance requires inertia parameters $\bar{\boldsymbol{z}}$ that are on the intersection of the null spaces of all the $\boldsymbol{X}_i$ matrices

$$\bar{\boldsymbol{z}} \in \ker(\boldsymbol{X}_i), \bar{\boldsymbol{z}} \in \ker(\bar{\boldsymbol{X}}_{k_{\max}}), \bar{\boldsymbol{z}} = \boldsymbol{N}\boldsymbol{y} \tag{47}$$

in which $\bar{\boldsymbol{X}}_{k_{\max}}^{\top} = \begin{bmatrix}\boldsymbol{X}_1^{\top} & \cdots & \boldsymbol{X}_{k_{\max}}^{\top}\end{bmatrix}$ is the collection of all regression matrices up to order $k_{\max}$. It should be emphasised that there is a finite $k_{\max}$, which makes the approach practically feasible. The columns of the $\boldsymbol{N}$ matrix form a basis that span this null space and therewith describe the full design space of the dynamically balanced inertia parameters. This $\boldsymbol{N}$ matrix is termed the *design space matrix* and may be found through numeric or symbolic null space algorithms such as Gauss-Jordan elimination or singular value decomposition. The corresponding design parameters are collected in $\boldsymbol{y}$. With this the complete set of dynamically balanced inertia parameters of any given nonsingular linkage may be found.

7. Partitioning and interpretation of the dynamic balance solution

The application of null space algorithms to the dynamic balance problem (Eq. 47) may result in a design space description that is strongly mixed in the inertia parameters, compromising structure and design intuition. To aid the designer, a partitioning of the design space with respect to the joint topology is presented alongside a multipole-rod representation (Fig. 1) of these partitions. We shall show that 6 types of inertia transfer matrices completely describe the design space of open-chain linkages. These inertia transfer matrices contain all inertia parameters that may be transferred between two hinged bodies, i.e. subtracted from one body and added to the other, without changing the momentum generated by the linkage. This partitioning will lead to a general description of the design space of open-chain linkages that, more importantly, also covers a large part of the design space of closed-loop linkages. Closed-loop linkages may be seen as a connection of multiple open chains. A balancing solution that is valid for open-chain linkages is therefore also valid for closed-chain linkages. Although the open-chain design space itself is always unfeasible, in combination with a closed-chain design space it allows for more feasible solutions as shown later in the examples.

7.1. Partitioning the design space of open-chain linkages

The dynamic balancing conditions of open-chain linkages (Eq. 31 and Eq. 37) are formulated in terms of aggregated mass matrices $\tilde{\boldsymbol{M}}_i$. Before presenting the general solution it may already be observed that solution to these equations will also be in terms the aggregated mass matrices. From these aggregated solutions each individual mass matrix can be found accordingly

$$\boldsymbol{M}_i = \tilde{\boldsymbol{M}}_i - \tilde{\boldsymbol{M}}_{i+1}, \boldsymbol{z}_i = \boldsymbol{N}_i \boldsymbol{y}_i - \boldsymbol{N}_{i+1}\boldsymbol{y}_{i+1}. \tag{48}$$

Therefore, the complete design space matrix $\boldsymbol{N}$ of an open chain (Eq. 47) may be partitioned as a band diagonal matrix

$$\begin{bmatrix}\boldsymbol{z}_1\\ \boldsymbol{z}_2\\ \vdots\\ \boldsymbol{z}_{n-1}\\ \boldsymbol{z}_n\end{bmatrix} = \begin{bmatrix}\boldsymbol{N}_1 & -\boldsymbol{N}_2 & & \cdots & \boldsymbol{0}\\ & \boldsymbol{N}_2 & -\boldsymbol{N}_3 & & \vdots\\ & & \ddots & \ddots & \\ \vdots & & & \boldsymbol{N}_{n-1} & -\boldsymbol{N}_n\\ \boldsymbol{0} & \cdots & & & \boldsymbol{N}_n\end{bmatrix}\begin{bmatrix}\boldsymbol{y}_1\\ \boldsymbol{y}_2\\ \boldsymbol{y}_3\\ \vdots\\ \boldsymbol{y}_{n-1}\\ \boldsymbol{y}_n\end{bmatrix} \tag{49}$$

in here the submatrix $\boldsymbol{N}_i$ describes all inertia parameters that can be exchanged between the two bodies connected by joint i without changing the dynamic behavior of the chain. These $\boldsymbol{N}_i$ submatrices are therefore termed inertia transfer matrices. In Section 7.3 it is shown that there exist actually 6 types of inertia transfer matrices depending on the type of joint and parallelism with the joint axes lower in the chain.

Table 1
The dimensions of the 6 inertia transfer matrices. Each joint i in a chain extends the design space depending on the type of joint; revolute (R), helical (H), or prismatic (P) and the alignment with all non-prismatic joints $j < i$ lower in the chain; a) skew or b) parallel. *With a prismatic joint, the prismatic joint direction applies $\boldsymbol{n}_i = \boldsymbol{n}_{i,\infty}$.

Joint type		R ($\lambda_i = 0$)	H (λ_i = finite)	P^* ($\lambda_i = \infty$)
Skew	$\boldsymbol{n}_j \nparallel \boldsymbol{n}_i$	3	1	6
Parallel	$\boldsymbol{n}_j \parallel \boldsymbol{n}_i$	5	4	7

It should be noted that a similar concept is used in the context of parameter identification to describe the set of unidentifiable inertia parameters [30,36]. Broadly speaking, inertia parameters are said to be unidentifiable if they do not contribute to the kinetic energy of the linkage. The dynamically balanced design space of open-chain linkages, as found here, is formed by unidentifiable inertia parameters as zero momentum in this case also implies zero kinetic energy. The inverse is not true in general. This also shows that the inertia parameters in this design space do not affect the required motor effort of the linkage.

7.2. Partitioning the design space of closed-chain linkages

We have already seen that closed-loop linkages can be converted into an open-chain equivalent by opening the loop. Therefore, the dynamic balance conditions, and hence the solutions, for open chains are also valid for closed-chain linkages. Yet, this is not necessarily the complete design space, since the loop-closure equations allow for dynamically balanced mass distributions that lie outside the design space of open-chain linages, i.e. $\text{rank}(\bar{\boldsymbol{X}}) \leq \text{rank}(\bar{\boldsymbol{W}})$. The design space of closed-chain linkages can therefore be partitioned into $\boldsymbol{N}_\text{O}$, dealing with the equivalent open-chains, termed *open-chain design space matrix*, and into a remainder $\boldsymbol{N}_\text{C}$ associated to the loop closure, termed *closed-chain design space matrix*

$$\boldsymbol{N} = \begin{bmatrix} \boldsymbol{N}_\text{O} & \boldsymbol{N}_\text{C} \end{bmatrix}, \boldsymbol{N}_\text{O} = \begin{bmatrix} \boldsymbol{N}_I & \cdots & \boldsymbol{N}_N \end{bmatrix}. \tag{50}$$

The open-chain equivalent design space matrix $\boldsymbol{N}_\text{O}$ is found by cutting the loops of a closed-loop linkage such that a set of N chains are found. The open-chain design space matrix $\boldsymbol{N}_I$ associated to chain I has the band-diagonal form of Eq. 49. The complete open-chain design space is the union of the open-chain design spaces of the chains into which the linkage may be decomposed. The open-chain design spaces of the individual chains are not necessarily disjoint, e.g. two design spaces bases $\boldsymbol{N}_I$ and $\boldsymbol{N}_{II}$ of a single loop may partly cover the same design space. This means that the rank of the open-chain design space is equal to, or smaller than, the sum of the rank of the individual open-chain design spaces. Furthermore it should be noted that the open-chain design space is invariant to where a loop is opened, although the basis might be different.

A meaningful closed-chain design space matrix is found by introducing a suitable test matrix $\boldsymbol{T}$, whose inertia parameters are not in the span of the open-chain design space. The null space basis $(\bar{\boldsymbol{X}}\boldsymbol{T})^\perp$ of the resulting higher-order momentum wrenches $\bar{\boldsymbol{X}}\boldsymbol{T}$ yields an interpretable design space matrix $\boldsymbol{N}_\text{C}$

$$\boldsymbol{N}_\text{C} = \boldsymbol{T}(\bar{\boldsymbol{X}}\boldsymbol{T})^\perp. \tag{51}$$

7.3. Interpretation of the design space via the concept of inertia transfer

In Section 5.3, it was shown that dynamic balance imposes two conditions on the aggregated mass matrices of open-chain linkages: Firstly, each aggregated mass matrix $\tilde{\boldsymbol{M}}_i$ should be chosen such that its IMW vanishes ($\tilde{\boldsymbol{M}}_i \boldsymbol{s}_i \equiv 0$). Secondly, the actuation of the corresponding joint q_i should not change the angular momentum generated by aany joint lower in the chain ($\partial / \partial q_i (\tilde{\boldsymbol{E}}_i)\boldsymbol{n}_j \equiv 0$ for all $j < i$). From the first condition three cases arise; an ISA of zero, finite or infinite pitch, while for the second condition two cases exist; either all axes up to $\boldsymbol{n}_i$ are parallel ($\boldsymbol{n}_j \parallel \boldsymbol{n}_i$ for all $j < i$) or at least one is skew ($\boldsymbol{n}_j \nparallel \boldsymbol{n}_i$ for $j < i$). This gives rise to 6 types of design space for 1-DOF lower kinematic pairs, and, consequently, 6 types of inertia transfer matrices $\boldsymbol{N}_i$ (Eq. 49). These are discussed now. For higher-DOF joints and joints in planar linkages a similar representation exist as shown subsequently.

7.3.1. Six inertia transfer matrices

Here, the multipole-rod representation of these six inertia transfer matrices are given (Fig. 2). In this notation the point mass, displacement and pure-inertia rod elements of the multipole-rod representation (Eq. 23) are respectively denoted by $\boldsymbol{z}_m(\boldsymbol{r})$, $\boldsymbol{z}_\delta(\boldsymbol{r}, \boldsymbol{n})$, and $\boldsymbol{z}_\eta(\boldsymbol{n})$. The dimensions of these inertia transfer matrices are in Table 1. Starting from a revolute joint, whose axis has no particular alignment, the six cases are discussed and interpreted.

$\boldsymbol{N}_{0,\nparallel}$ The inertia transfer matrix associated to a revolute joint ($\lambda = 0$) — whose joint axis is skew ($\nparallel$) with respect to one or more preceding revolute or helical joints — comprise of three inertia parameters. These three parameters can be freely exchanged (added to one and subtracted from the other) between the two bodies hinged by this joint without

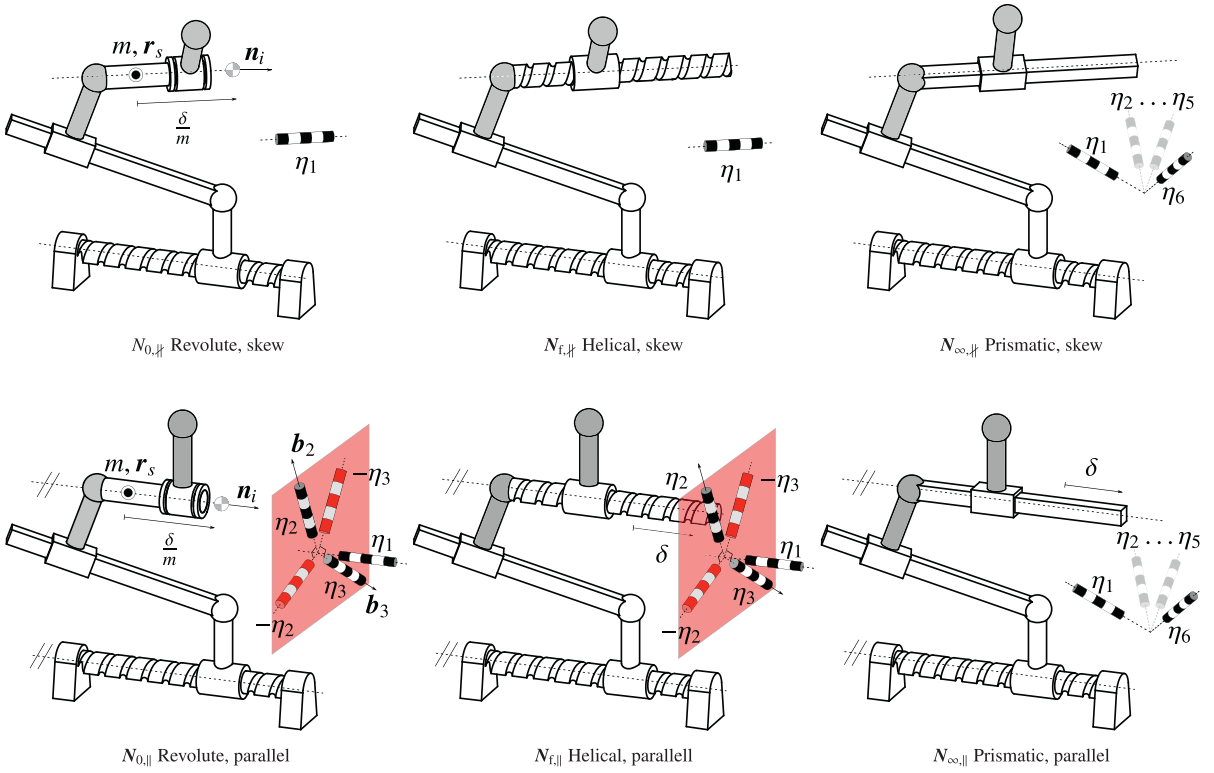

Fig. 2. The interpretation of the six sets of inertia parameters that can be exchanged between the two (grey) bodies attached to joint i (subtracted from one and added to the other) without changing the dynamic behaviour of the chain as a whole. These six cases arise from the three types of 1-DOF lower pairs, and parallelism with all preceding revolute and helical joints. The orientation of the preceding prismatic joints have no influence. It should be noted that for clarity sake the effect of the displacement δ on the MOIs is not shown, as it can be compensated by, or absorbed in η_1. Since the pure-inertia rods have no application point, they are displayed at an arbitrary location.

affecting the momentum generated by the chain as a whole. These parameters are: 1) a point mass $\boldsymbol{z}_m$ on the joint axis $\boldsymbol{r}_s$, 2) a displacement of this point $\boldsymbol{z}_\delta$ in the direction of the joint axis $\boldsymbol{n}$, 3) a pure-inertia rod η in the direction of the joint axis $\boldsymbol{n}$. The corresponding inertia transfer matrix therefore reads

$$\boldsymbol{N}_{0,\nparallel} = \begin{bmatrix} \boldsymbol{z}_m(\boldsymbol{r}_s) & \boldsymbol{z}_\delta(\boldsymbol{n}, \boldsymbol{r}_s) & \boldsymbol{z}_\eta(\boldsymbol{n}) \end{bmatrix}. \tag{52}$$

The reason for these three inertia transfers is that the actuation of a joint with a point mass m anywhere on its axis $\boldsymbol{r}_s$ does not induce any linear or angular momentum, nor does it change the IWM of lower joints (Eq. 37), since and equal and opposite point mass is attached to the connecting body. This yields the design freedoms $\boldsymbol{z}_m$ and $\boldsymbol{z}_\delta$. The third design freedom, a pure-inertia rod η, generates no angular momentum as it is aligned with the joint axis. This alignment also makes sure that the rotation of this pure-inertia rod by the joint will not cause a change in the inertia matrix felt by the lower joints.

Any other exchange of mass or inertia between the two bodies connected by this joint will either change the momentum generated by this joint or by the joints lower in the chain.

$\boldsymbol{N}_{0,\parallel}$ When the revolute joint ($\lambda = 0$) is parallel with respect to all preceding revolute and helical joints, two additional parameters are obtained, in comparison to $\boldsymbol{N}_{0,\nparallel}$. These parameters are two perpendicular pairs of pure-inertia rods. All these all four rods are on a single plane perpendicular to $\boldsymbol{n}$. These pure-inertia rod are of opposite magnitude in a pair wise manner (Fig. 2).

These four additional pure-inertia rods allow for a modification of the inertia tensor without changing the dynamics of the chain. The first of the pure-inertia rod pairs η_2 is in the direction of $\boldsymbol{b}_2$, which is perpendicular to $\boldsymbol{n}$. The angular momentum induced by $\boldsymbol{b}_2$ is cancelled by an equal and negative pure-inertia rod in a direction perpendicular to both $\boldsymbol{n}$ and $\boldsymbol{b}_2$. This also holds for a second pair η_3 with corresponding $\boldsymbol{b}_3$. This additional pure-inertia rods arise since their common plane which is perpendicular to $\boldsymbol{n}$ is not changing by actuation of the joints lower in the chain. The inertia transfer matrix is therefore parametrized according to

$$\boldsymbol{N}_{0,\parallel}(\boldsymbol{s}) = \begin{bmatrix} \boldsymbol{z}_m(\boldsymbol{r}_s) & \boldsymbol{z}_\delta(\boldsymbol{n}, \boldsymbol{r}_s) & \boldsymbol{z}_\eta(\boldsymbol{n}) & \boldsymbol{z}_\eta(\boldsymbol{b}_2) - \boldsymbol{z}_\eta(\boldsymbol{n} \times \boldsymbol{b}_2) & \boldsymbol{z}_\eta(\boldsymbol{b}_3) - \boldsymbol{z}_\eta(\boldsymbol{n} \times \boldsymbol{b}_3) \end{bmatrix} \tag{53}$$

$\boldsymbol{N}_{\mathrm{f},\nparallel}$ For a helical ($\lambda = \text{finite}$), non-parallel joint any point mass will generate a linear momentum through its pitching motion such that its inertia transfer matrix only contains a pure-inertia rod in the direction of the joint axis. The displacement ($\boldsymbol{z}_\delta$) would cause a pose dependent inertia matrix and non-constant IWMs associated to the lower joints. The sole inertia change is therefore

$$\boldsymbol{N}_{\mathrm{f},\nparallel} = \boldsymbol{z}_\eta(\boldsymbol{n}) \tag{54}$$

$\boldsymbol{N}_{\mathrm{f},\parallel}$ When a helical joint is parallel to all preceding revolute and parallel joints it has a similar inertia transfer space as $\boldsymbol{N}_{0,\parallel}$ (Eq. 53) with the sole difference that the mass should therefore equate to zero as the pitching motion would generate a linear momentum. The displacement ($\boldsymbol{z}_\delta$) on the other hand does not induce linear momentum and therefore remains

$$\boldsymbol{N}_{\mathrm{f},\parallel} = \begin{bmatrix} \boldsymbol{z}_\delta(\boldsymbol{n}, \boldsymbol{r}_s) & \boldsymbol{z}_\eta(\boldsymbol{n}) & \boldsymbol{z}_\eta(\boldsymbol{b}_2) - \boldsymbol{z}_\eta(\boldsymbol{n} \times \boldsymbol{b}_2) & \boldsymbol{z}_\eta(\boldsymbol{b}_3) - \boldsymbol{z}_\eta(\boldsymbol{n} \times \boldsymbol{b}_3) \end{bmatrix} \tag{55}$$

$\boldsymbol{N}_{\infty,\nparallel}$ The inertia transfer of a prismatic joint ($\lambda = \infty$) whose joint axis is not aligned with all preceding revolute or helical joint axes has a size 6, since its $\boldsymbol{E}$ can be selected freely. As these moments and products of inertia will not induce angular momentum (and are constant) they can be selected as desired. Here this choice is parameterized by 6 pure-inertia rods

$$\boldsymbol{N}_{\infty,\nparallel} = \begin{bmatrix} \boldsymbol{z}_\eta(\boldsymbol{b}_1) & \cdots & \boldsymbol{z}_\eta(\boldsymbol{b}_6) \end{bmatrix}. \tag{56}$$

$\boldsymbol{N}_{\infty,\parallel}$ When the prismatic joint ($\lambda = \infty$) is aligned with preceding zero and finite pitch joints it gains a displacement $\boldsymbol{z}_\delta$ in the direction of the joint axis, leading to an inertia transfer matrix with size 7

$$\boldsymbol{N}_{\infty,\parallel} = \begin{bmatrix} \boldsymbol{z}_\delta(\boldsymbol{n}_\infty, \boldsymbol{n}_\infty) & \boldsymbol{z}_\eta(\boldsymbol{b}_1) & \cdots & \boldsymbol{z}_\eta(\boldsymbol{b}_6) \end{bmatrix}. \tag{57}$$

7.3.2. Multi-DOF joints

This approach also holds for multi-DOF joints that can locally be modelled as a serial connection of 1-DOF joints, e.g., cylindrical, planar, universal or spherical joints. These multi-DOF joints can the transmit inertia parameters that are common in the lower kinematic pair analogue. For example, a cylindrical joint can be modelled as prismatic and a revolute joint in series such that its inertia transfer matrix is the intersection of the image of $\boldsymbol{N}_0$ and $\boldsymbol{N}_\infty$, which is the inertia transfer associated to a helical joint $\boldsymbol{N}_\mathrm{f}$. Depending on the parallelism with the joints lower in the chain, either type is to be selected. A planar joint is serial connection of two prismatic joints such that its inertia transfer is $\boldsymbol{N}_\infty$. Universal and spherical joints locally behave as a serial connection of multiple non-parallel, intersecting revolute joints. The associated inertia transfer is therefore a point mass $\boldsymbol{z}_m(\boldsymbol{r})$ on the intersection point $\boldsymbol{r}$ of these axes. We assume here that the joint itself does not contain intermediate bodies with mass or inertia.

7.3.3. Joints in planar linkages

In the planar case only zero and infinite pitch ISA exist. Therefore, three types of inertia transfer matrices appear, 1) the ISA is revolute and therefore automatically parallel to all other revolute joints, 2) the ISA and all lower ISA are prismatic joints or 3) the ISA is prismatic but at least one of the lower joints is a revolute joint

$$\boldsymbol{N}_0 = \boldsymbol{z}_m(\boldsymbol{r}_s), \boldsymbol{N}_{\infty,\parallel} = \begin{bmatrix} \boldsymbol{z}_\delta(\boldsymbol{n}_\infty) & \boldsymbol{z}_\eta \end{bmatrix}, \boldsymbol{N}_{\infty,\nparallel} = \boldsymbol{z}_\eta \tag{58}$$

In the first case, the point mass should be on the revolute joint and the MOI around that point should be zero. In the second case, the body solely translates, therefore the mass should be zero and the first and second moments of mass are free, as parameterized by a displacement and a pure-inertia rod. In the third case, when the ISA under inspection is prismatic and one or more lower joints are revolute, this displacement will causes a changing MOI associated to the rotation of the lower joints. This the displacement should therefore be zero.

With this description of the inertia transfer matrices $\boldsymbol{N}_i$ of common joints, the dynamically balanced design space of any open-chain linkage may be obtained. Also for closed-chain linkages, the open-chain equivalent design space matrix $\boldsymbol{N}_\mathrm{O}$ is completely determined, generalizing [23] to spatial linkages. It should be noted that open linkages cannot be dynamically balanced without addition of counter-mechanisms. This can also be established from the inertia transfer matrices as none of them permit both a positive mass and positive MOIs. Therefore, a specific $\boldsymbol{N}_\mathrm{C}$ is required to render a feasible dynamically balanced design space. The existence of this additional design space is found on a case-by-case basis in the next section.

8. Case studies

The higher-order dynamic balance approach is illustrated here with case studies of a serial 6-DOF robot, a planar 4*R* four-bar linkage, and a 3-*RSR* mechanism. In all cases an interpretation of the closed-chain design space bases $\boldsymbol{N}_\mathrm{C}$ will be given, if present.

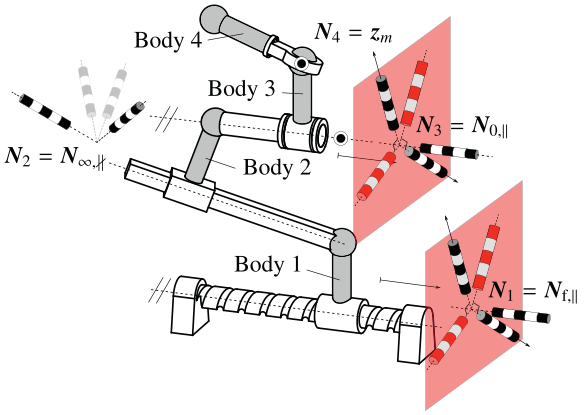

Fig. 3. The 16 dynamically balanced design parameters of the *HPRS* 6-DOF serial chain. Each of the four joints permits a transfer of inertia parameters $\boldsymbol{N}_i$.

8.1. Serial 6-DOF robot

Here we study a 6-DOF robot to show how the open-chain design space matrix is found. We consider a *HPRS*-robot (Fig. 3) of which the first joint axis remains parallel to the third joint axis $\boldsymbol{n}_1 = \boldsymbol{n}_3$. The second, prismatic joint has no particular alignment. The fourth, spherical joint is modelled as three intersecting twists $\boldsymbol{s}_4$, $\boldsymbol{s}_5$, and $\boldsymbol{s}_6$ with no intermediate bodies. Therefore this linkages consists of four bodies in total. The zeroth-order regression matrix and the associated design space matrix become

$$\boldsymbol{W}_0 = \begin{bmatrix} \begin{bmatrix}\boldsymbol{s}_1*\end{bmatrix} & \begin{bmatrix}\boldsymbol{s}_1*\\ \boldsymbol{s}_2*\end{bmatrix} & \begin{bmatrix}\boldsymbol{s}_1*\\ \boldsymbol{s}_2*\\ \boldsymbol{s}_3*\end{bmatrix} & \begin{bmatrix}\boldsymbol{s}_1*\\ \boldsymbol{s}_2*\\ \boldsymbol{s}_3*\\ \boldsymbol{s}_4*\\ \boldsymbol{s}_5*\\ \boldsymbol{s}_6*\end{bmatrix} \end{bmatrix}, \boldsymbol{N} = \begin{bmatrix} \boldsymbol{N}_1 & -\boldsymbol{N}_2 & & \\ & \boldsymbol{N}_2 & -\boldsymbol{N}_3 & \\ & & \boldsymbol{N}_3 & -\boldsymbol{N}_4 \\ & & & \boldsymbol{N}_4 \end{bmatrix} \tag{59}$$

This zeroth-order regression matrix has $\text{rank}(\boldsymbol{W}_0) = 23$. Through application of the algorithm presented in Section 6, it is found that the regression matrix terminates at $k_{\max} = 1$ with $\text{rank}(\tilde{\boldsymbol{W}}_1) = 24$ leaving $n_b \times 10 - \text{rank}(\tilde{\boldsymbol{W}}_1) = 16$ design parameters free.

This can be explained by further investigation of $\boldsymbol{W}_1$. It is found that only one partial derivative $(\partial/\partial q_2(\hat{\boldsymbol{h}}_1) = \partial/\partial q_2(\tilde{\boldsymbol{M}}_2)\boldsymbol{s}_1)$ leads to additional dynamic balancing conditions in comparison to $\boldsymbol{W}_0$. All other derivatives are 'covered' by the zeroth-order conditions. Therefore, the only relevant rows of the first-order regression matrix are

$$\boldsymbol{W}_1 = -\begin{bmatrix}\boldsymbol{0}_{36\times 10} & \begin{bmatrix}\text{ad}(\boldsymbol{s}_2)\boldsymbol{s}_1*\end{bmatrix} + \text{ad}(\boldsymbol{s}_2)^\top\begin{bmatrix}\boldsymbol{s}_1*\end{bmatrix} & \cdots & \begin{bmatrix}\text{ad}(\boldsymbol{s}_2)\boldsymbol{s}_1*\end{bmatrix} + \text{ad}(\boldsymbol{s}_2)^\top\begin{bmatrix}\boldsymbol{s}_1*\end{bmatrix}\end{bmatrix} \tag{60}$$

It should be noted that the first 10 columns are zero, due to $\partial/\partial q_2(\boldsymbol{M}_1) = \boldsymbol{0}$. Since $\boldsymbol{s}_2$ is not aligned with $\boldsymbol{s}_1$, the actuation of q_2 will cause a displacement of the aggregated COM of bodies 2, 3, and 4, leading to a change of the aggregated mass matrix felt by $\boldsymbol{s}_1$. As the other joints are either aligned ($\boldsymbol{n}_1 = \boldsymbol{n}_3$) or spherical ($S$, Section 7.3.2), no additional constraints are placed. The corresponding inertia transfer matrices in Eq. 59 are therefore

$$\boldsymbol{N}_1 = \boldsymbol{N}_{f,\|}(\boldsymbol{s}_1), \boldsymbol{N}_2 = \boldsymbol{N}_{\infty,\nparallel}(\boldsymbol{s}_2), \boldsymbol{N}_3 = \boldsymbol{N}_{0,\|}(\boldsymbol{s}_3), \boldsymbol{N}_4 = \boldsymbol{z}_m(\boldsymbol{r}_4) \tag{61}$$

The first joint is a helical joint fixed to the base such that it inertia transfer matrix has $\text{rank}(\boldsymbol{N}_{f,\|}) = 4$ (Eq. 55). The second joint is a prismatic joint whose axis is not parallel to joint 1 such that is inertia transfer matrix has $\text{rank}(\boldsymbol{N}_{\infty,\nparallel}) = 6$ (Eq. 56). In fact, if only the zeroth-order balancing condition would be taken into account $\boldsymbol{N}_2$ would gain an additional 'displacement' and it would be $\boldsymbol{N}_{\infty,\|}$. The revolute joint, joint 3, is parallel and stays parallel to the preceding finite pitch ISA (joint 1) such that it has an inertia transfer matrix of $\text{rank}(\boldsymbol{N}_{0,\|}) = 5$ (Eq. 53). The spherical joint is seen as the intersection of three perpendicular revolute joints such that it solely transmits a point mass at the intersection point $\boldsymbol{z}_m(\boldsymbol{r}_4)$. This leads to a total design freedom of $\text{rank}(\boldsymbol{N}) = 16$, which again is in agreement with the order of the regression matrix $\tilde{\boldsymbol{W}}_{k_{\max}}$ that is found with the presented algorithm.

This shows that the complete design space is found through a combination of the inertia transfer matrices that are readily available by inspecting the joint types and alignment of these joints in the chain.

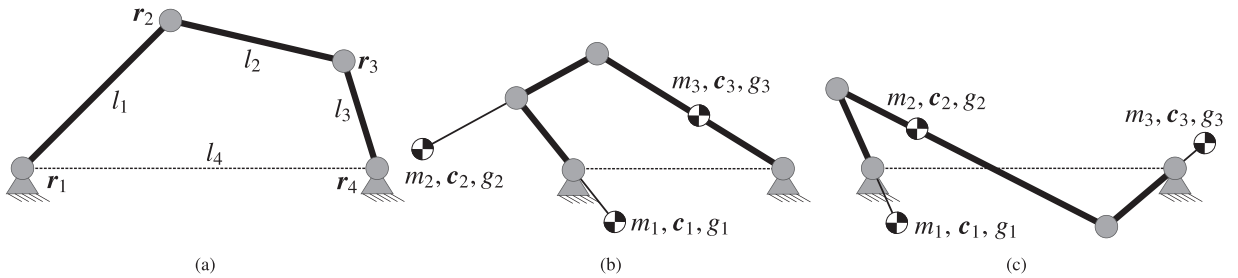

Fig. 4. (a) The kinematic definition of the planar four-bar linkage, with the two dynamically balanced types (b) the kite and (c) the antiparallelogram (adapted from [8]).

8.2. Planar four-bar linkage

The planar 4*R* four-bar linkage is a classical example in the dynamic balance literature. Although studied for decades [3,37,38], a solution that does not rely on additional counter-mechanisms was not found until the year 2000 by Ricard and Gosselin [8]. Thereafter, this linkage has been used as dynamic balancing module to obtain 3-DOF and 6-DOF dynamically balanced mechanisms [9]. Here, this linkage is studied to show that the current method replicates the results from literature.

The linkage consist of four revolute joints at $\boldsymbol{r}_1$ up to $\boldsymbol{r}_4$. The first and last joints are attached to the base (Fig. 4). The moving links have lengths l_1, l_2, and l_3 and the base length is l_4. We analyse this linkage by cutting the third link between joint 3 and 4. Two kinematic branches *I* and *II* are obtained, consisting of joint 1, 2, and 3, and joint 4, respectively. Therefore, the open-chain equivalent design space matrix becomes

$$\boldsymbol{N}_{\mathrm{O}} = \begin{bmatrix} \boldsymbol{N}_I & \boldsymbol{N}_{II} \end{bmatrix}, \boldsymbol{N}_I = \begin{bmatrix} \boldsymbol{N}_1 & -\boldsymbol{N}_2 & \boldsymbol{0} \\ \boldsymbol{0} & \boldsymbol{N}_2 & -\boldsymbol{N}_3 \\ \boldsymbol{0} & \boldsymbol{0} & \boldsymbol{N}_3 \end{bmatrix}, \boldsymbol{N}_{II} = \begin{bmatrix} \boldsymbol{0} \\ \boldsymbol{0} \\ -\boldsymbol{N}_4 \end{bmatrix} \tag{62}$$

Since all joints are planar revolute joints, the inertia transfer matrices consist of a point mass at the joint location (Eq. 58), i.e. $\boldsymbol{N}_i = \boldsymbol{N}_0 = \boldsymbol{z}_m(\boldsymbol{r}_i)$. This shows that the inertia parameter of link 3, at which the cut has been made, will lie on the span of $\boldsymbol{N}_3$ and $\boldsymbol{N}_4$. The loop opening can also be performed at another link resulting in another basis for the same null space. Therefore, $\mathrm{rank}(\boldsymbol{N}_{\mathrm{O}}) = 4$.

Through application of the higher-order derivatives algorithm, the $\bar{\boldsymbol{X}}$-matrix is obtained. Inspection of the rank $\bar{\boldsymbol{X}}$-matrix reveals that in the general case, this matrix has a maximum rank of $\mathrm{rank}(\bar{\boldsymbol{X}}_{k_{\max}}) = 8$ and requires $k_{\max} = 3$ derivatives to reach this limit. Since there are 12 inertia parameters, this linkage has a design freedom $\mathrm{rank}(\boldsymbol{N}) = 4$. This shows that with the loop-opening method the complete design space of the general four-bar linkage has been found. This open-chain equivalent design space has no feasible solutions, since the addition of a positive point mass to one link requires a negative point mass on the connecting link. A feasible link with a positive MOI requires at least two positive point masses, which is not supported by this general solution.

Fortunately, there exist two special kinematic conditions in which the dimension of the design space increases and the linkage permits feasible dynamically balanced solutions [8,14]. These are the anti-parallelogram ($l_1 = l_3,\ l_2 = l_4$) and the kite-type four-bar linkage ($l_1 = l_2,\ l_3 = l_4$), as shown in Fig. 4. In both cases, the base link has to be wider than two equal moving links. Here we study only the anti-parallelogram case, for which the rank of the $\bar{\boldsymbol{X}}$ matrix drops to $\mathrm{rank}(\bar{\boldsymbol{X}}) = 7$ and the design space is extended with a basis

$$\boldsymbol{N}_{\mathrm{C}}^{\top} = \begin{bmatrix} \boldsymbol{z}_\eta^{\top} & -\boldsymbol{z}_\eta^{\top} & \boldsymbol{z}_\eta^{\top} \end{bmatrix} \tag{63}$$

This may be interpreted as three pure-inertia rods in which the inertia connected to the coupler is opposite to the other two [39]. This solution arises since the links of the linkage follow a linear relation on the angular velocities $\boldsymbol{\omega}_1 - \boldsymbol{\omega}_2 + \boldsymbol{\omega}_3 = 0$ [40]. The solution is parameterized by y_1 up to y_5. The first four parameters deal with the open-chain equivalent $\boldsymbol{N}_{\mathrm{O}}$, while the variable y_5 is associated to $\boldsymbol{N}_{\mathrm{C}}$. The resulting body masses and local MOIs become

$$m_i = y_i - y_{i+1}, g_i = l_i^2\left(1 - \frac{y_i}{m_i}\right)y_i + (-1)^{i+1}y_5. \tag{64}$$

From the mass positivity condition (Eq. 19) it follows that the design parameters should be selected decreasingly through the chain

$$y_1 > y_2 > y_3 > y_4 \tag{65}$$

The positivity of the MOI places upper and lower bounds on the choice of y_5

$$y_5 > l_1^2\left(1 - \frac{y_1}{m_1}\right)y_1, y_5 < l_2^2\left(1 - \frac{y_2}{m_2}\right)y_2, y_5 > l_1^2\left(1 - \frac{y_3}{m_3}\right)y_3. \tag{66}$$

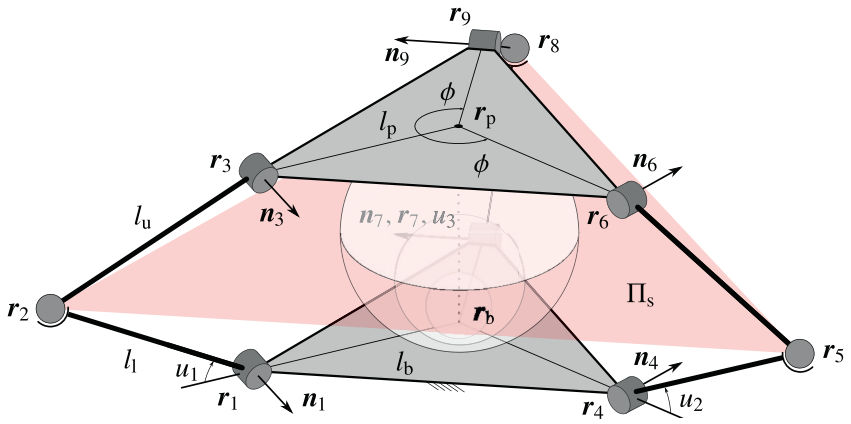

Fig. 5. The kinematic definition of the 3-*RSR*. During motion the end-effector stays tangential to an expanding sphere touching the platform centre and the base centre [41]. This mechanism is mirror symmetric with respect to a plane Π_s passing through the spherical joints $\boldsymbol{r}_2$, $\boldsymbol{r}_5$, and $\boldsymbol{r}_8$..

A similar result emerges for the kite-type four-bar linkage, with the sole difference that the crank and the coupler have an equal positive moment of inertia whereas the rocker has a negative moment of inertia. With this example we have shown that dynamic balancing results from literature could be replicated using the proposed higher-order dynamic balancing method. Furthermore we have shown an example in which the loop opening solution aids in interpreting the whole dynamic balance solution and the feasibility conditions. The special kinematic cases, as found by Moore and Gosselin [14], may also be derived from rank reduction of $\bar{\boldsymbol{X}}$-matrix, but this lies outside the scope of this paper.

8.3. 3-RSR spatial parallel mechanism

To show that this procedure also holds for multi-DOF linkages, we investigate a symmetric 3-*RSR* mechanism [41]. In this section we will show that the design space of the 3-*RSR* does not contain feasible designs when considering the whole of its workspace. Fortunately, it permits a dynamically balanced solution for 2-DOF movements over three planes of symmetry.

8.3.1. Kinematics of the 3-RSR mechanism

The 3-*RSR* under investigation (Fig. 5) consist of 3 arms whose upper and lower links are of equal length $l_u = l_l$. The platform and the base have identical dimensions $l_b = l_p$. The first arm consist of two revolute joints 1 and 3, respectively hinged at the base at $\boldsymbol{r}_1$ and at the platform at $\boldsymbol{r}_3$. Their joint axes $\boldsymbol{n}_1$ and $\boldsymbol{n}_3$ are co-linear in the reference configuration. The spherical joint, which connect link 1 and 2, is located at $\boldsymbol{r}_2$. Arms 2 and 3 are similar yet rotated with ϕ and $-\phi$ around the vertical axis. The platform is link 7. The three base joints are chosen to be the independent coordinates u_1, u_2, and u_3. Throughout motion the mechanism is mirror symmetric with respect to a plane Π_s passing through the three *S*-joints [41,42]. Due to this symmetry, the platform of this robot remains tangential ($\boldsymbol{r}_p$) to a variable sized sphere whose south pole is fixed at the origin ($\boldsymbol{r}_b$) of the robot.

8.3.2. General dynamic balance solution

Similar to previous example, the open-chain equivalent design space is found by cutting the three kinematic loops at the platform leaving three *RSR* chains, respectively consisting of joints 1–3, 4–6 and 7–9. The corresponding design space matrix is

$$\boldsymbol{N}_O = \begin{bmatrix} \boldsymbol{N}_1 & -\boldsymbol{N}_2 & \boldsymbol{0} & & & & & & \\ \boldsymbol{0} & \boldsymbol{N}_2 & -\boldsymbol{N}_3 & & & & & & \\ & & & \boldsymbol{N}_4 & -\boldsymbol{N}_5 & \boldsymbol{0} & & & \\ & & & \boldsymbol{0} & \boldsymbol{N}_5 & -\boldsymbol{N}_6 & & & \\ & & & & & & \boldsymbol{N}_7 & -\boldsymbol{N}_8 & \boldsymbol{0} \\ & & & & & & \boldsymbol{0} & \boldsymbol{N}_8 & -\boldsymbol{N}_9 \\ \boldsymbol{0} & \boldsymbol{0} & \boldsymbol{N}_3 & \boldsymbol{0} & \boldsymbol{0} & \boldsymbol{N}_6 & \boldsymbol{0} & \boldsymbol{0} & \boldsymbol{N}_9 \end{bmatrix} \tag{67}$$

with

$$\boldsymbol{N}_1 = \boldsymbol{N}_{0,\parallel}(\boldsymbol{s}_1), \quad \boldsymbol{N}_2 = \boldsymbol{z}_m(\boldsymbol{r}_2), \quad \boldsymbol{N}_3 = \boldsymbol{N}_{0,\nparallel}(\boldsymbol{s}_3) \tag{68}$$

$$\boldsymbol{N}_4 = \boldsymbol{N}_{0,\parallel}(\boldsymbol{s}_4), \boldsymbol{N}_5 = \boldsymbol{z}_m(\boldsymbol{r}_5), \boldsymbol{N}_6 = \boldsymbol{N}_{0,\nparallel}(\boldsymbol{s}_6) \tag{69}$$

$$\boldsymbol{N}_7 = \boldsymbol{N}_{0,\parallel}(\boldsymbol{s}_7), \boldsymbol{N}_8 = \boldsymbol{z}_m(\boldsymbol{r}_8), \boldsymbol{N}_9 = \boldsymbol{N}_{0,\nparallel}(\boldsymbol{s}_9) \tag{70}$$

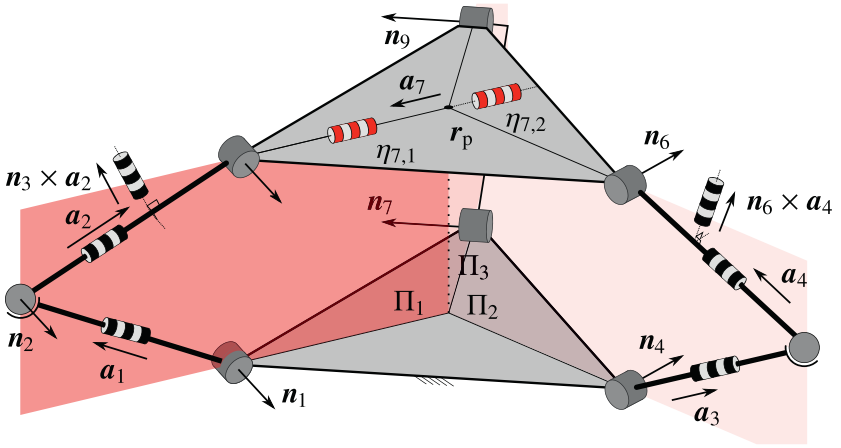

Fig. 6. The 3-RSR mechanism can be dynamically balanced for motion over three additional planes of symmetry. For movement over the first plane, indicated by Π_1, one may add a pure-inertia rods to the first arm and a negative pure-inertia rod to the platform $\eta_{7,1}$. Also on arms 2 and 3 extra pure-inertia rods may be placed in combination with a negative pure-inertia rod on the platform $\eta_{7,2}$. Although not shown here, arm 3 has to be identical to arm 2. Later the balance for the other planes Π_2 and Π_3 is solved.

The base revolute joints have fixed axes while the platform joints have moving axes, giving rise to their respective inertia transfer matrices. Since a spherical joint (S) is instantaneously equivalent to three perpendicular intersecting revolute joints, its inertia transfer matrix $\boldsymbol{N}_i$ is a point mass at the joint location $\boldsymbol{r}_i$, for $i = 2$, 5 and 8. This yields a open-chain equivalent design space with a rank of $3 \times (5 + 1 + 3) = 27$. The $\bar{\boldsymbol{X}}$-matrix, which is found through the presented algorithm, terminates at $k_{\max} = 2$ and has a rank$(\bar{\boldsymbol{X}}_{k_{\max}}) = 43$. With 7 moving links and 70 inertia parameters to determine, it is shown that the complete design space is given by the open-chain equivalent design space ($70 = 43 + 27$) and no closed-chain design space exists. Therefore, additional counter-mechanisms are required for the dynamic balance of this 3-*RSR* mechanism.

8.3.3. Dynamic balance for 2-DOF motion on planes of symmetry

Fortunately, the mechanism can be dynamically balanced when only a part of the workspace is considered. Here we will investigate the case when the platform centre $\boldsymbol{r}_\mathrm{p}$ moves on another plane Π_1 that normal to joint axis $\boldsymbol{n}_1$ (Fig. 6). This occurs when the two other base joints move in unison $u_2 = u_3$. During this 2-DOF motion the mechanism maintains kinematic mirror symmetry with respect to this plane. Later on, we will show that this permits a symmetric mass distribution over the 3 arms and the platform such that the mechanism is also dynamically balanced when moving over the other two planes of symmetry, i.e Π_2 when $u_1 = u_3$ and Π_3 when $u_1 = u_2$.

When the mechanism's end-effector is constrained to move on plane Π_1, the rank of the regression matrix drops by 8 to rank$(\bar{\boldsymbol{X}}_{k_{\max}}) = 35$, yielding a design space of dimension 35. A part of this enlarged design space can be explained by the fact that the S-joint of arm 1 now behaves as a revolute joint ($\boldsymbol{n}_1 \| \boldsymbol{n}_2 \| \boldsymbol{n}_3$) enlarging the open-chain design space by 6. Now the first arm's inertia transfer matrices (Eq.) become

$$\boldsymbol{N}_2 = \boldsymbol{N}_{0,\|}(\boldsymbol{s}_2), \boldsymbol{N}_3 = \boldsymbol{N}_{0,\|}(\boldsymbol{s}_3) \tag{71}$$

Furthermore, an additional closed-chain design space of rank 2 appears, similar to that of the kite-type planar four-bar linkage (Section 8.2). When the first joint (u_1) is actuated and the others ($\dot{u}_2 = \dot{u}_3 = 0$) are fixed, the first arm and the platform moves as a kite-type four-bar linkage due to the mirror symmetry with respect to the plane Π_s through the S-joints (Fig. 5). Due to this symmetry for all poses, the angular velocities of the bodies have a particular linear relation $\boldsymbol{\omega}_1 + \boldsymbol{\omega}_2 = \boldsymbol{\omega}_7$. The first column of the closed-chain design space matrix is therefore

$$\boldsymbol{N}_{\mathrm{C},1}^\top = \begin{bmatrix} \boldsymbol{z}_\eta^\top(\boldsymbol{a}_1) & 1/2(\boldsymbol{z}_\eta^\top(\boldsymbol{a}_2) + \boldsymbol{z}_\eta^\top(\boldsymbol{n}_3 \times \boldsymbol{a}_2)) & \boldsymbol{0}_{1\times 40} & \eta_{7,1}\boldsymbol{z}_\eta^\top(\boldsymbol{a}_7) \end{bmatrix}, \qquad \eta_{7,1} = -1 \tag{72}$$

For the second 'symmetric' DOF $u_2 = u_3$ a second mirror symmetry is of importance; the mirror symmetry with respect to the plane Π_1 perpendicular to $\boldsymbol{n}_1$ and passing through the centre of the base (Fig. 6). This is encoded in an angular velocity relation $\boldsymbol{\omega}_1 + \boldsymbol{\omega}_2 + \boldsymbol{\omega}_7 = \boldsymbol{\omega}_3 + \boldsymbol{\omega}_4 + \boldsymbol{\omega}_5 + \boldsymbol{\omega}_6$. Since arms 2 and 3 move in mirror symmetry with this plane, the second column is found to be

$$\boldsymbol{N}_{\mathrm{C},2}^\top = \begin{bmatrix} \boldsymbol{0}_{1\times 20} & \boldsymbol{z}_\eta^\top(\boldsymbol{a}_3) & 1/2(\boldsymbol{z}_\eta^\top(\boldsymbol{a}_4) + \boldsymbol{z}_\eta^\top(\boldsymbol{n}_6 \times \boldsymbol{a}_4)) & \boldsymbol{z}_\eta^\top(\boldsymbol{a}_5) & 1/2(\boldsymbol{z}_\eta^\top(\boldsymbol{a}_6) + \boldsymbol{z}_\eta^\top(\boldsymbol{n}_9 \times \boldsymbol{a}_6)) & \eta_{7,2}\boldsymbol{z}_\eta^\top(\boldsymbol{a}_7) \end{bmatrix} \tag{73}$$

with

$$\eta_{7,2} = -1/2(\cos(2\phi) + 3) \tag{74}$$

So arms 2 and 3 move in opposite directions with respect to this additional symmetric plane Π_1 (Fig. 6), cancelling the angular momentum components in this plane. In the perpendicular direction ($\boldsymbol{n}_1$) the angular momentum is counter-acted by the negative pure-inertia rod of the platform.

Table 2
Geometric parameters of the simulated 3-*RSR* mechanisms.

Name	Symbol	Value	Unit
Base width	l_b	3.00	[m]
Platform width	l_p	3.00	[m]
Lower arm length	l_l	1.00	[m]
Upper arm length	l_u	1.00	[m]
Arm angle	ϕ	$3/2\pi$	[rad]

8.3.4. Feasibility conditions

The resulting 35-dimensional solution space contains a range of feasible solutions. These solutions compensate the negative pure-inertia rods ($\eta_{7,1}$ and $\eta_{7,2}$) of the moving platform by addition of positive point masses to the shoulder, i.e the $\boldsymbol{z}_m(\boldsymbol{r}_i)$ in the corresponding inertia transfer matrix $\boldsymbol{N}_i$, for $i = 3$, 6, and 9. We will illustrate this on a mechanisms with a rotational symmetric base and platform ($\phi = 2/3\pi$). For demonstration purposes we reduce the rather large design space by choosing 1) all 3 arms to have an equal mass distribution, 2) the COMs to be inline with the arms, 3) an axisymmetric platform, and 4) the principal axis to be aligned with the links.

The remaining parameters may be chosen freely as long as the mass and inertia feasibility conditions are satisfied (Eq. 19). The mass of the links become the sum of the point mass transfers

$$m_1 = m_3 = m_5 = y_1 - y_6, m_2 = m_4 = m_6 = y_6 - y_{11}, m_7 = 3y_{11}. \tag{75}$$

The principal MOIs follow from the summation of the pure-inertia rods. Here the first principal axis is $\boldsymbol{n}_1$, the second is $\boldsymbol{a}_1$, and the third is $\boldsymbol{a}_1 \times \boldsymbol{n}_1$. The principal MOIs of the first link are

$$g_{1,1} = y_{34} + l_l^2 y_1 \left(1 - \frac{y_1}{m_1}\right), g_{1,2} = y_3 - y_5 - y_8, g_{1,3} = g_{1,1} + g_{1,2} + 2y_5. \tag{76}$$

For the second link the principal axes are oriented similarly; in the directions of $\boldsymbol{n}_3$, $\boldsymbol{a}_2$, and $\boldsymbol{n}_3 \times \boldsymbol{a}_2$, respectively

$$g_{2,1} = y_{34} + l_u^2 y_6 \left(1 - \frac{y_6}{m_2}\right), g_{2,2} = y_8 - y_{13} + \frac{1}{2} y_{34}, g_{2,3} = g_{2,1} + g_{2,2} - y_{34}. \tag{77}$$

The MOIs of the links of the other 2 arms are equal $\boldsymbol{g}_1 = \boldsymbol{g}_3 = \boldsymbol{g}_5$ and $\boldsymbol{g}_2 = \boldsymbol{g}_4 = \boldsymbol{g}_5$. The MOIs of the platform are formed by the closed-chain design space basis y_{34}, the added point masses at the shoulder y_{11}, the inertia transfer y_{13} over the connecting joints (i.e. in the direction of $\boldsymbol{n}_i$ for $i = 3$, 6, and 9), and the modification of by inertia transfer over the first chain y_{14}. The first principal MOI is around $\boldsymbol{a}_7$, the second around $\boldsymbol{n}_3$ and in the third out-of-plane direction $\boldsymbol{n}_3 \times \boldsymbol{a}_7$

$$g_{7,1} = \frac{3}{2}\left(l_p^2 y_{11} + y_{13}\right) - \frac{1}{2} y_8 - y_{14}, g_{7,2} = \frac{3}{2}\left(l_p^2 y_{11} + y_{13} - y_8\right) - \frac{9}{4} y_{34}, g_{7,3} = g_{7,1} + g_{7,2} + 2y_{14}. \tag{78}$$

Now the platform is chosen axisymmetric $g_{7,1} = g_{7,2}$ by setting

$$y_8 = y_{14} - \frac{9}{4} y_{34.} \tag{79}$$

This axisymmetric solution extends the dynamically balanced motion over the two other planes of mirror symmetry Π_2 and Π_3, which are perpendicular to the base joints $\boldsymbol{n}_4$ and $\boldsymbol{n}_7$, respectively. It should be noted that the resulting mechanism is force balanced for its complete workspace.

By invoking the feasibility conditions (Eq. 19) we obtain the following set of feasibility conditions for the 3-*RSR* mechanism moving in a single plane Π_1. It should be noted that several shadowing inequality conditions have been removed

$$0 < y_{11} < y_6 < y_1, \qquad y_{13} < y_8 < y_3, \qquad y_5 < 0, \qquad y_{14} < 0, \tag{80}$$

$$2l_u^2 \frac{y_6 y_{11}}{m_2} < y_{34}, 0 < y_{34} + y_5 + l_u^2 y_1 \left(1 - \frac{y_1}{m_1}\right), \qquad 0 < l_p^2 y_{11}^2 + y_{13} + y_{14} - \frac{3}{2} y_{34.} \tag{81}$$

It should be noted that similar feasibility conditions, yet more complex, can be obtained for the full 35-dimensional design. Furthermore, the satisfaction of the feasibility conditions does not guarantee a practical implementation of the resulting balance solution. The solution, for example, may require very slender links or centres of mass at a long distance from the joint, which may be hard to realize in practice.

8.3.5. Numerical study

Based on these findings a geometry and design parameters $\boldsymbol{y}$ are selected for simulation (Table 2, and 3). The corresponding mass distribution is found in Table 4. In here the COM location of the arms are defined as $\boldsymbol{c}_i = \boldsymbol{r}_i - c_i \boldsymbol{a}_i$. Whereas c_i denote the distance to the connecting joint (Fig. 7). The COM of platform is at the centre of the platform $\boldsymbol{c}_7 = \boldsymbol{r}_p$.

Simulations of this mechanism in a multibody software package confirm the dynamically balanced mass distribution by showing shaking forces and moments that are effectively zero for movement over the three symmetric planes (Fig. 8). The remaining shaking force and moments are attributed to round off errors.

Table 3
The design parameters of the dynamically balanced 3-*RSR* mechanism as used in the numerical example.

Subspace			Range	Value				
Arm 1	$\boldsymbol{N}_I$	$\boldsymbol{N}_1$	$\boldsymbol{y}_{1\ldots5}$	2.00	0.00	−2.10	−0.05	−0.30
		$\boldsymbol{N}_2$	$\boldsymbol{y}_{6\ldots10}$	0.40	0.00	−2.30	−0.05	0.00
		$\boldsymbol{N}_3$	$\boldsymbol{y}_{11\ldots15}$	0.20	0.00	−2.40	−0.05	0.00
Arm 2	$\boldsymbol{N}_{II}$	$\boldsymbol{N}_4$	$\boldsymbol{y}_{16\ldots20}$	2.00	0.00	0.20	0.00	−0.30
		$\boldsymbol{N}_5$	y_{21}	0.40				
		$\boldsymbol{N}_6$	$\boldsymbol{y}_{22\ldots24}$	0.20	0.00	−0.10		
Arm 3	$\boldsymbol{N}_{III}$	$\boldsymbol{N}_7$	$\boldsymbol{y}_{25\ldots29}$	2.00	0.00	0.20	0.00	−0.30
		$\boldsymbol{N}_8$	y_{30}	0.40				
		$\boldsymbol{N}_9$	$\boldsymbol{y}_{31\ldots33}$	0.20	0.00	−0.10		
Closed-chain	$\boldsymbol{N}_C$		$\boldsymbol{y}_{34\ldots35}$	1.00	1.00			

Table 4
The resulting masses, centres of mass (COMs) locations and moments of inertia (MOIs) for the different links of the 3-*RSR* as used in simulation.

Name	Symbol	1	2	3	4	5	6	7	Unit
Mass	m_i	1.60	0.20	1.60	0.20	1.60	0.20	0.60	kg
COM	c_i	0.25	1.00	0.25	1.00	0.25	1.00	0.00	m
MOI 1	$g_{i,1}$	0.40	0.20	0.40	0.20	0.40	0.20	0.30	kg m^2
MOI 2	$g_{i,2}$	0.50	0.60	0.50	0.60	0.50	0.60	0.30	kg m^2
MOI 3	$g_{i,3}$	0.50	0.60	0.50	0.60	0.50	0.60	0.50	kg m^2

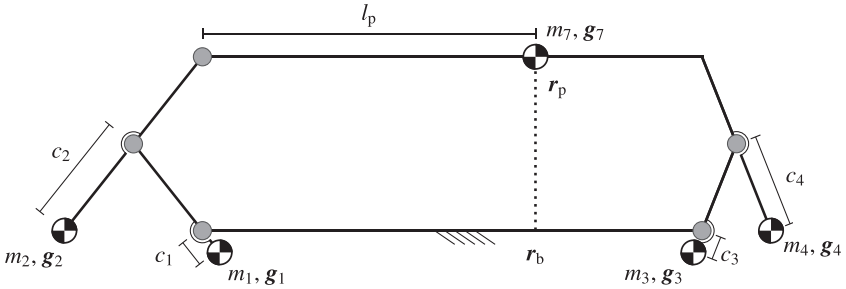

Fig. 7. A side view (of Π_1) of the dynamically balanced 3-*RSR* as used in the simulation.

9. Discussion

The proposed method achieves dynamic balance by eliminating a finite but sufficient number of higher-order partial derivatives of the momentum wrench. This results in the necessary and sufficient balancing conditions since the momentum is an analytic function outside of singularities. Therefore, if the higher-order derivatives of such an analytic function are zero, the function itself is identically equal to zero and no shaking forces and moments are exerted on the base.

In this paper it is shown (Section 5.3) that for open-chain linkages up to two derivatives ($k_{\max} = 2$) are required to obtain the necessary and sufficient conditions for dynamic balance. For closed-chain linkages such a general upper-bound on the number of derivatives is not found. Therefore, each case requires an inspection of the $\tilde{\boldsymbol{X}}$-matrix, as done in the examples. Although a constant rank of the $\tilde{\boldsymbol{X}}$-matrix for higher orders it is a strong indicator, verification of the balancing solution is still formally required, for example by numerical simulation. Furthermore, different linkages, but also different geometries lead to different $k_{\max}$ values. For example, for the general planar four-bar $k_{\max} = 3$ while for the (anti–)parallelogram geometry $k_{\max} = 2$.

By selection of a sub-matrix of the $\tilde{\boldsymbol{X}}$-matrix, a larger design space may appear and the conditions for exact dynamic balance are relaxed in favour of other requirements. For example, force balance only may be obtained by selecting the relevant rows. Alternatively, approximate balancing may be obtained by satisfying only derivatives up to a certain order, yielding dynamic balance in a neighbourhood of the reference pose. Path balance may be obtained by only regarding paths or planes through the reference pose, as shown by the 3-*RSR* example. This method therefore generalizes the result of [26].

The feasibility conditions (Eq. 19) dictate whether or not a desired mass distribution can be constructed. To check the feasibility, an eigenvalue problem is to be solved. The non-linear nature of the eigenvalue problem however, prevents a closed-form treatment for arbitrary linkages. Currently this study is done on an individual basis. Yet, for simple linkages the partitioning and multipole-rod representation allowed for an interpretation and feasibility study without eigenvalues decomposition. Furthermore, even though some of the linkages studied here have no feasible design space, the complete

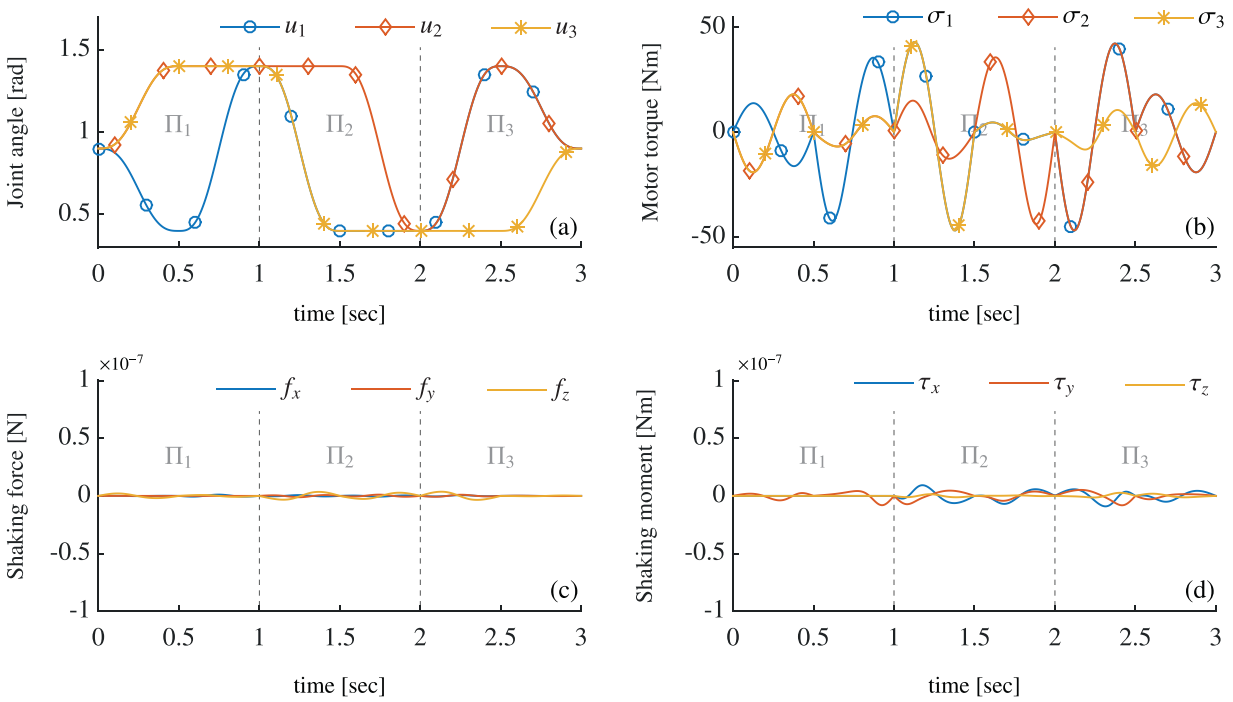

Fig. 8. A simulation of the 3-*RSR* mechanism moving on a trajectory (a) over the three symmetric planes (Π_i) confirm dynamic balance as the resulting shaking forces (c) and shaking moments (d) effectively zero. The remaining shaking forces and moments are attributed to computation accuracy. For comparison, (b) shows the torques σ_i that the motors exert on the base.

characterization of the design space is expected to assist in the selection of the most favourable application dependent solution, i.e. with minimal motor torque and/or minimal number of counter-mechanisms.

10. Conclusion

This paper presented a higher-order dynamic balancing method that yields and solves the necessary and sufficient dynamic balance conditions of open- or closed-chain, planar or spatial linkages in nonsingular configurations. This method relies on a recursive algorithm to obtain the higher-order derivatives of the rigid body momentum equations up to an arbitrary order. In the parameter-linear form these higher-order derivatives furnish the dynamic balance conditions that arise from a rank deficiency of the regression matrix. This enables generic null space procedures to yield the complete set of dynamically balanced inertia parameters, i.e. the complete dynamically balanced design space of a given linkage. It was shown that for open-chain linkages, derivatives up to the second order yield the necessary and sufficient balance conditions. For such linkages the partial derivatives of higher orders will pose no new dynamic balance conditions. For closed-chain linkages such an upper bound was found per case. Partitioning and interpretation of the design space of open-chain linkages was presented based on the concept of inertia transfer. Six inertia transfer matrices where found that, depending on the alignment of the joints and the types of joints in the chain, allow for an exchange of inertia parameters without affecting the momentum generated by the linkage as a whole. For general closed-loop linkages this open-chain equivalent design space fully describe the dynamically balanced design space, resulting in non-feasible designs due to negative masses or moments of inertia. Fortunately, in special cases a the loop-closure permits a larger design space enabling feasible and constructable balance solutions. Also, a larger design space is found when only a part of the workspace is to be dynamically balanced. For the 3-*RSR* mechanism, for instance, three dynamically balanced planes of symmetric 2-DOF motion were obtained without resorting to counter-mechanisms.

With this method a systematic, closed-form dynamic balance algorithm is presented that provides a uniform framework to study linkages that require no or a minimal number of counter-mechanisms, paving the way for the dynamic balancing of high-speed robots.

Declaration of Competing Interest

None.

Acknowledgements

The second author acknowledges that this work has been partially supported by the Austrian COMET-K2 program of the Linz Center of Mechatronics (LCM).

Appendix. Multivariate matrix derivatives using Kronecker product

The higher-order partial derivatives of matrices are managed in this paper with the use of the Kronecker product [33]. In this appendix the Kronecker product notation and some elementary properties are listed along with the application to the

Table A1
List of symbols.

Symbol	Description	Reference
$\begin{bmatrix}\bullet\times\\ \bullet*\end{bmatrix}$	Skew symmetric matrix Regression matrix form of the parameter-linear form	Eq. 9 Eq. 42
$\bullet\otimes\bullet$	Kronecker product	Eq. A.1
$\bar{\bullet}$	Collection of matrices	Eq. 8
$\tilde{\bullet}$	Aggregated form, sum of masses, MOIs etc. of the higher links	Eq. 31
$\boldsymbol{\alpha}$, $\boldsymbol{\beta}$	Multi-index	Eq. 12, 30
δ	The displacement multipole element	Fig. 1, Eq. 23
η	The pure-inertia rod multipole element	Fig. 1, Eq. 23
$\boldsymbol{\xi}$	Angular momentum vector	Eq. 16
Π	Plane of kinematic mirror symmetry	Fig. 6
$\boldsymbol{\omega}$	Angular velocity vector	Eq. 6
$\boldsymbol{c}$	Position of the centre of mass (COM)	Eq. 17
$\boldsymbol{C}$	Basis matrix expressing the solution of the first order solution to the loop closure equation	Eq. 8
$\mathrm{D}^{\boldsymbol{\alpha}}(\bullet)$	Repeated derivatives according to multi-index $\boldsymbol{\alpha}$	Eq. A.3
$\mathrm{D}^{k}(\bullet)$	Collection of all partial derivatives of order k	Eq. A.4
$\boldsymbol{e}$	Vector with the moments and products of inertia	Eq. 17
$\boldsymbol{E}$	Moment of inertia matrix	Eq. 17
f	Loop closure constraint equations	Eq. 8
$\boldsymbol{g}$	Principle moments of inertia	Eq. 18
$\boldsymbol{h}$, $\hat{\boldsymbol{h}}$	Momentum wrench and instantaneous momentum wrench, respectively	Eq. 16, 20
$\boldsymbol{H}_i^j$	Transformation matrix from frame i to frame j	Eq. 9
$\mathrm{Ad}(\boldsymbol{H})$	Adjoint transformation matrix	Eq. 10
$\mathrm{ad}(\boldsymbol{t})$	Adjoint twist matrix	Eq. 11
$\boldsymbol{I}_n$	Identity matrix of size n	Eq. 17
$\boldsymbol{J}$	Jacobian of the open-chain equivalent mechanism	Eq. 8
$\boldsymbol{K}$	First order loop closure constraints	Eq. 8
m	Mass	Eq. 17
$\boldsymbol{M}$	Mass matrix	Eq. 17
$\boldsymbol{n}$	Unit vector in direction of screw axis	Eq. 7
$\boldsymbol{N}$, $\boldsymbol{N}_I$, $\boldsymbol{N}_\mathrm{O}$, $\boldsymbol{N}_\mathrm{C}$	Design space matrix of respectively the complete mechanism, of chain I, of the open-chain equivalent mechanism and of the loop closure	Eq. 47, 50
$\boldsymbol{N}_i$, $\boldsymbol{N}_0$, $\boldsymbol{N}_f$, $\boldsymbol{N}_\infty$, $\boldsymbol{N}_\parallel$, $\boldsymbol{N}_\nparallel$	Inertia transfer matrix, respectively associated to joint i, to a zero, finite, or infinite pitch joint, to a joint that is parallel or not with the preceding joints	Eq. 49, 52–57, Fig. 2
$\boldsymbol{p}$	Linear momentum vector	Eq. 16
$\boldsymbol{q}$	Joint coordinate vector of an open-chain (equivalent) mechanism	Eq. 7
$\boldsymbol{s}$	Instantaneous screw axis (ISA)	Eq. 7
$\boldsymbol{t}$	Twist vector	Eq. 6
$\boldsymbol{u}$	Vector of minimal coordinates	Eq. 8
$\boldsymbol{v}$	Velocity vector	Eq. 6
$\boldsymbol{W}$	Regression matrix of an open-chain (equivalent) mechanism	Eq. 43
$\boldsymbol{X}$	Regression matrix of a closed-chain mechanism	Eq. 46
$\boldsymbol{y}$	Vector of design variables of the dynamically balanced mass distribution	Eq. 47, 50
$\boldsymbol{z}$	Vector of the inertia parameters in the parameter-linear form	Eq. 41
$\boldsymbol{z}_m$, $\boldsymbol{z}_\delta$, $\boldsymbol{z}_\eta$	Parameter-linear form of the elements of the multi-pole rod representation, respectively the mass, displacement and pure-inertia rod	Eq. 23, 41

bookkeeping of the higher-order partial derivatives. The differences between the repeated higher-order partial derivatives $\mathrm{D}^{\boldsymbol{\alpha}}_{\boldsymbol{x}}(\boldsymbol{A})$ and the collection of higher-order partial derivatives $\mathrm{D}^{k}_{\boldsymbol{x}}(\boldsymbol{A})$ are highlighted.

The Kronecker product is defined as the collection of the element-wise multiplication of all elements in the respective matrices. Consider the following set of matrices: $\boldsymbol{A} \in \mathbb{R}^{n\times m}, \boldsymbol{B} \in \mathbb{R}^{p\times q}$

$$\boldsymbol{A}\otimes\boldsymbol{B} = \begin{bmatrix} a_{11}\boldsymbol{B} & \cdots & a_{1m}\boldsymbol{B} \\ \vdots & \ddots & \vdots \\ a_{n1}\boldsymbol{B} & \cdots & a_{nm}\boldsymbol{B} \end{bmatrix}. \tag{A.1}$$

The vectorization of a triple matrix product is written by means of the Kronecker product

$$\mathrm{vec}(\boldsymbol{ABC}) = (\boldsymbol{C}^{\top}\otimes\boldsymbol{A})\mathrm{vec}(\boldsymbol{B}). \tag{A.2}$$

A set of nested higher-order partial derivatives is denoted with a vector in the superscript $\mathrm{D}^{\boldsymbol{\alpha}}_{\boldsymbol{x}}(\boldsymbol{A}) = \partial^k/(\partial x_1^{\alpha_1}\cdots\partial x_n^{\alpha_n})$. Consider for example the following repeated partial derivatives

$$\frac{\partial}{\partial x_1}\frac{\partial^3}{\partial x_2^3}\frac{\partial^2}{\partial x_5^2}(\boldsymbol{A}) = \mathrm{D}^{\boldsymbol{\alpha}}_{\boldsymbol{x}}(\boldsymbol{A}) \text{with} \boldsymbol{\alpha} = [1,3,0,0,2]. \tag{A.3}$$

The $\boldsymbol{\alpha}$-vector is an ordered multi-index corresponding to $\boldsymbol{x}$. The total order is given by $\sum_i \alpha_i = |\boldsymbol{\alpha}|$. These repeated higher-order partial derivatives form the elements (rows and submatrices) of the collection of higher-order partial derivatives, i.e. $\mathrm{D}^{k}_{\boldsymbol{x}}(\boldsymbol{A})$ is formed by all nested partial derivatives with respect to $\boldsymbol{\alpha}$ for which $|\boldsymbol{\alpha}| = k$.

The collection of partial derivatives of a given vector $\boldsymbol{a}$ with respect to $\boldsymbol{x} \in \mathbb{R}^r$ are organized according to

$$\mathrm{D}_{\boldsymbol{x}}(\boldsymbol{a}) = \begin{bmatrix} \frac{\partial}{\partial x_1}(\boldsymbol{a}) & \ldots & \frac{\partial}{\partial x_r}(\boldsymbol{a}) \end{bmatrix}, \quad \mathrm{D}_{\boldsymbol{x}}(\mathrm{D}_{\boldsymbol{x}}(\boldsymbol{a})) = \begin{bmatrix} \mathrm{D}_{\boldsymbol{x}}\left(\frac{\partial}{\partial x_1}(\boldsymbol{a})\right) & \ldots & \mathrm{D}_{\boldsymbol{x}}\left(\frac{\partial}{\partial x_r}(\boldsymbol{a})\right) \end{bmatrix}. \tag{A.4}$$

This is extended to the partial derivatives of a matrix $\boldsymbol{A} = \begin{bmatrix}\boldsymbol{a}_1 & \ldots & \boldsymbol{a}_m\end{bmatrix}$, which are organized according

$$\mathrm{D}_{\boldsymbol{x}}(\boldsymbol{A}) = \begin{bmatrix} \mathrm{D}_{\boldsymbol{x}}(\boldsymbol{a}_1) & \cdots & \mathrm{D}_{\boldsymbol{x}}(\boldsymbol{a}_m) \end{bmatrix}, \quad \mathrm{D}^2_{\boldsymbol{x}}(\boldsymbol{A}) = \mathrm{D}_{\boldsymbol{x}}(\mathrm{D}_{\boldsymbol{x}}(\boldsymbol{A})) = \begin{bmatrix} \mathrm{D}^2_{\boldsymbol{x}}(\boldsymbol{a}_1) & \cdots & \mathrm{D}^2_{\boldsymbol{x}}(\boldsymbol{a}_m) \end{bmatrix}. \tag{A.5}$$

The following entities may be found for the derivatives of matrices $\boldsymbol{A}(\boldsymbol{x}) \in \mathbb{R}^{n\times m}$, $\boldsymbol{B}(\boldsymbol{x}) \in \mathbb{R}^{m\times q}$ and $\boldsymbol{x} \in \mathbb{R}^r$

Product rule For a matrix product the following derivative holds

$$\mathrm{D}_{\boldsymbol{x}}(\boldsymbol{AB}) = \mathrm{D}_{\boldsymbol{x}}(\boldsymbol{A})(\boldsymbol{B}\otimes\boldsymbol{I}_r) + \boldsymbol{A}\mathrm{D}_{\boldsymbol{x}}(\boldsymbol{B}). \tag{A.6}$$

Chain rule For matrix function $\boldsymbol{A}(\boldsymbol{b}(\boldsymbol{c}))$ with nested variables $\boldsymbol{b}$ and $\boldsymbol{c}$ the derivative becomes

$$\mathrm{D}_{\boldsymbol{c}}(\boldsymbol{A}(\boldsymbol{b}(\boldsymbol{c}))) = \mathrm{D}_{\boldsymbol{b}}(\boldsymbol{A})(\boldsymbol{I}_m\otimes\mathrm{D}_{\boldsymbol{c}}(\boldsymbol{b})). \tag{A.7}$$

Kronecker product The derivative of the Kronecker product is written using the permutation matrix $\boldsymbol{P}_{q,r}$ [33]

$$\mathrm{D}_{\boldsymbol{x}}(\boldsymbol{A}\otimes\boldsymbol{B}) = (\mathrm{D}_{\boldsymbol{x}}(\boldsymbol{A})\otimes\boldsymbol{B})(\boldsymbol{I}_m\otimes\boldsymbol{P}_{q,r}) + \boldsymbol{A}\otimes\mathrm{D}_{\boldsymbol{x}}(\boldsymbol{B}). \tag{A.8}$$

Matrix inversion The derivative of a matrix inverse becomes

$$\mathrm{D}_{\boldsymbol{x}}\left(\boldsymbol{A}^{-1}\right) = -\boldsymbol{A}^{-1}\mathrm{D}_{\boldsymbol{x}}(\boldsymbol{A})(\boldsymbol{A}^{-1}\otimes\boldsymbol{I}_r). \tag{A.9}$$

A recursive application of these equations allow for the extension of these derivatives up to arbitrary order.

References

[1] G.G. Lowen, F.R. Tepper, R.S. Berkof, Balancing of linkages an update, Mech Mach Theory 18 (3) (1983) 213–220.
[2] V.H. Arakelian, M.R. Smith, Shaking force and shaking moment balancing of mechanisms: a historical review with new examples, J. Mech. Des. 127 (2) (2005) 334–338.
[3] R.S. Berkof, Complete force and moment balancing of inline four-bar linkages, Mech Mach Theory 8 (3) (1973) 397–410.
[4] J.L. Herder, C.M. Gosselin, A counter-rotary counterweight (CRCW) for light-weight dynamic balancing, in: Proceedings of ASME DETC, 2004, pp. 1–9.
[5] C. Bagci, Shaking force balancing of planar linkages with force transmission irregularities using balancing idler loops, Mech Mach Theory 14 (4) (1979) 267–284.
[6] Y.Q. Yu, Research on complete shaking force and shaking moment balancing of spatial linkages, Mech Mach Theory 22 (I) (1987) 27–37.
[7] S. Briot, I.A. Bonev, C.M. Gosselin, V. Arakelian, Complete shaking force and shaking moment balancing of planar parallel manipulators with prismatic pairs, in: Proceedings of the Institution of Mechanical Engineers, Part K: Journal of Multi-body Dynamics, 223, 2009, pp. 43–52.
[8] R. Ricard, C.M. Gosselin, On the development of reactionless parallel manipulators, in: ASME - DETC2000 MECH-14098, 1, 2000, pp. 1–10. Baltimore, Maryland
[9] Y. Wu, C.M. Gosselin, Synthesis of reactionless spatial 3-DOF and 6-DOF mechanisms without separate counter-rotations, Int J Rob Res 23 (6) (2004) 625–642.
[10] O. Fischer, Theoretische Grundlagen für eine Mechanik der lebenden Körper, Teubner, Leipzig, 1906.
[11] V. Van der Wijk, J.L. Herder, Synthesis method for linkages with center of mass at invariant link point Pantograph based mechanisms, Mech Mach Theory 48 (2011) 15–28.
[12] V. Van der Wijk, S. Krut, F. Pierrot, J.L. Herder, Design and experimental evaluation of a dynamically balanced redundant planar 4-RRR parallel manipulator, Int J Rob Res 32 (6) (2013) 744–759.
[13] B. Moore, J. Schicho, Two methods for force balancing of bennett linkages, in: Computational Kinematics, 2009, pp. 241–248.
[14] B. Moore, J. Schicho, C.M. Gosselin, Determination of the complete set of shaking force and shaking moment balanced planar four-bar linkages, Mech Mach Theory 44 (7) (2009) 1338–1347.
[15] V. Van der Wijk, Shaking-moment balancing of mechanisms with principal vectors and momentum, Frontiers of Mechanical Engineering 8 (1) (2013) 10–16.

[16] J. Wiederrich, B. Roth, Momentum balancing of four-bar linkages, Journal of Engineering for Industry 98 (4) (1976) 1289–1295.
[17] C.M. Gosselin, Note sur les conditions d'équilibrage de Berkof et Lowen, in: Congrès Canadien de Mécanique Appliquée, 1, 1997, pp. 497–498.
[18] M.L. Husty, An algorithm for solving the direct kinematics of general Stewart-Gough platforms, Mech Mach Theory 31 (4) (1996) 365–379.
[19] R.S. Berkof, G.G. Lowen, A new method for completely force balancing simple linkages, Journal of Engineering for Industry 91 (1) (1969) 21–26.
[20] R.E. Kaufman, G.N. Sandor, Complete force balancing of spatial linkages, Journal of Engineering for Industry 93 (2) (1971) 620–626.
[21] N.X. Chen, The complete shaking force balancing of a spatial linkage, Mech Mach Theory 19 (2) (1984) 243–255.
[22] I.S. Kochev, General method for full force balancing of spatial and planar linkages by internal mass redistribution, Mech Mach Theory 22 (4) (1987) 333–341.
[23] Z. Ye, M. Smith, Complete balancing of planar linkages by an equivalence method, Mech Mach Theory 29 (5) (1994) 701–712.
[24] C.M. Gosselin, B. Moore, J. Schicho, Dynamic balancing of planar mechanisms using toric geometry, J Symb Comput 44 (9) (2009) 1346–1358.
[25] B. Moore, J. Schicho, C.M. Gosselin, Dynamic balancing of spherical 4R linkages, J Mech Robot 2 (2) (2010) 021002.
[26] J.J. De Jong, J. Van Dijk, J.L. Herder, A screw based methodology for instantaneous dynamic balance, Mech Mach Theory 141 (2019) 267–282.
[27] J.J. De Jong, A. Müller, J.L. Herder, Higher-order Taylor approximation of finite motions in mechanisms, Robotica 37 (7) (2019) 1190–1201.
[28] W. Khalil, F. Bennis, Symbolic calculation of the base inertial parameters of closed-loop robots, Int J Rob Res 14 (2) (1995) 112–128.
[29] A. Codourey, E. Burdet, A body-oriented method for finding a linear form of the dynamic equation of fully parallel robots, in: International Conference on Robotics and Automation, Albuquerque, 1997, pp. 1612–1618.
[30] J. Ros, X. Iriarte, V. Mata, 3D Inertia transfer concept and symbolic determination of the base inertial parameters, Mech Mach Theory 49 (2012) 284–297.
[31] R.W. Brockett, Robotic manipulators and the product of exponentials formula, Mathematical Theory of Networks and Systems SE - 9 58 (1984) 120–129.
[32] A. Müller, An overview of formulae for the higher-order kinematics of lower-pair chains with applications in robotics and mechanism theory, Mech Mach Theory 142 (2019) 103459.
[33] W.J. Vetter, Matrix calculus operations and Taylor expansions, Society for Industrial and Applied Mathematics 15 (2) (1973) 352–369.
[34] R.S. Ball, A treatise on the theory of screws, Cambridge University Press, UK, Cambridge, 1900.
[35] J. Selig, Applying screw theory to robot dynamics, J. Appl. Math. Mech. 55 (3) (1991) 159–167.
[36] P.M. Wensing, G. Niemeyer, J.-J.E. Slotine, Observability in inertial parameter, Identification (2017) 1808.04099.
[37] G.G. Lowen, R.S. Berkof, Survey of investigations into the balancing of linkages, Journal of Mechanisms 3 (4) (1969) 221–231.
[38] C. Bagci, Complete shaking force and shaking moment balancing of link mechanisms using balancing idler loops, J. Mech. Des. 104 (2) (1982) 482–493.
[39] J.J. De Jong, Y.Q. Wu, M. Carricato, J.L. Herder, A pure-inertia method for dynamic balancing of symmetric planar mechanisms, in: Advances in Robot Kinematics, 5, 2018, pp. 1–8.
[40] S. Briot, V. Arakelian, Complete shaking force and shaking moment balancing of in-line four-bar linkages by adding a class-two RRR or RRP Assur group, Mech Mach Theory 57 (2012) 13–26.
[41] I. Bonev, Geometric analysis of parallel mechanisms, 2003 Ph.D. thesis.
[42] Y.Q. Wu, M. Carricato, Symmetric subspace motion generators, IEEE Trans. Rob. 34 (3) (2018) 716–735.